Shared binding sites for the chromosomal architectural protein Su(Hw) mediate physical interactions between *Drosophila* TAD boundaries.

Wenfan Ke[1,2], Miki Fujioka[4], Brendan Wang[2], Tiffany Park[1], Li Zhang[5], Amina Kurbidaeva[6], Yuri Pritykin[2,3], James B Jaynes[4], and Paul Schedl[1]

1) Department of Molecular Biology, Princeton University, Princeton, NJ, USA 08540
2) Lewis Sigler Institute of Integrative Genomics, Princeton University, Princeton, NJ, USA 08540
3) Department of Computer Science, Princeton University, Princeton, NJ, USA, 08540
4) Department of Biochemistry and Molecular Biology, Thomas Jefferson University, Philadelphia, PA, USA, 19107
5) The key laboratory of Dairy Science of Education Ministry, Northeast Agricultural University, Harbin, Heilongjiang, P.R. China, 150030
6) Center for Genomics and Systems Biology, New York University, New York, NY, USA, 10003

Abstract

Loop extrusion has been clearly shown to be insufficient as a mechanism to explain TAD formation, leaving a large gap in our understanding of how the specificity of TAD boundary interactions and inter-TAD chromosomal interactions are determined. Many TAD binding proteins have been implicated in boundary interactions, including the *gypsy* transposon boundary binding protein Su(Hw). How these proteins generate the often specific and orientation-dependent boundary interactions that underpin chromosomal architecture is largely unknown. Here, we investigate the role of the single Su(Hw) binding site located in each of the boundaries that flank the Drosophila *eve* locus, *homie* and *nhomie*. We show that Su(Hw), which binds hundreds of sites throughout the Drosophila genome, plays a large role in the highly

selective and orientation-specific interactions of *homie* and *nhomie*. Despite its outsized role in the binding strength and stability of these interactions, other boundary binding proteins are implicated as the primary determinants of the specificity of the interactions. These studies provide an important example of the need to more fully investigate how strength and specificity of TAD boundary interactions are separately encoded in this important class of genome architectural elements.

Introduction

Studies on lampbrush chromosomes were the first to suggest that the key organizing principle for chromosomes in animals is the subdivision of the chromatin into a series of topologically independent loops (now called TADs) that extend from the main chromosomal axis (Gall and Callan, 1962; Callan, 1986; Callan, 1987). Each lampbrush chromosome has a stereotypic pattern of loops, and in most loops there is only a single actively transcribed gene. The loops are anchored to the main axis of the chromosome, and the anchors pull apart when the chromosomes are stretched (Callan, 1986, 1987). Since then, a variety of approaches have shown that TADs are pervasive features of chromosomes in multicellular organisms (Rao et al., 2014; Dekker and Heard, 2015; Eagen et al., 2015; Stadler et al., 2017; Hsieh et al., 2021; Krietenstein et al., 2020; Goel et al., 2023; Dolstein et al., 2025). In flies, TADs range in size from only a few kb to over 100 kb, while recent MicroC and Region Capture MicroC (RCMC) studies indicate that the scale is similar in mammals. The arrangement of TADs along a given chromosome tends to be invariant and is largely, but not completely, independent of cell type or developmental stage (Bing et al. 2024; Ke et al., 2024; Dolstein et al., 2025).

This regular and heritable organization is generated by a special class of *cis*-acting elements called boundaries or insulators. Boundary elements were first discovered and have been most fully characterized in *Drosophila*; however, similar elements have been identified in other species (Ghirlando et al., 2012; Ghirlando and Felsenfeld, 2016; Chetverina et al., 2017; Matthews and White 2019; Cavaleiro et al., 2 021). Boundary elements in flies consist of one or more large (>150 bp) nuclease hypersensitive regions and can span DNA sequences of up to 1.5 kb in length. These nuclease-hypersensitive regions are targets for a large and diverse collection of DNA binding proteins that have been implicated in boundary function (Parkhurst et al., 1988; Gasner et al., 1999; Golovin et al., 2007; Maksimento et al., 2015; Zolotarev et al, 2016; Fedotova et al., 2017; Chetverina et al. 2021; Bonchuk et al., 2021; Bonchuk et al., 2023). Of these, the most prevalent class are polydactyl C2H2 zinc finger proteins {e.g., CTCF, Zw5, Su(Hw), Pita, Zipic, Clamp, Zad1}(Bonchuk et al., 2021; Fedotova et al., 2017). Other boundary factors include several BEN domain proteins (Insv, Elba1-2), GAF, Ibf1/2, BEAF, CP190 and the 31 Mod(mdg4) isoforms (Zhao et al., 1995; Bonchuk et al., 2011; Aoki et al., 2012; Dai et al. 2013; Cuartero et al., 2013; Avva and Hart, 2016). As there are over 200 mostly uncharacterized polydactyl C2H2 zinc finger proteins, including some 70 proteins that have the

Zad homodimerization domain, encoded in the fly genome (Bonchuk et al., 2021), it is likely that a large number of chromosomal architectural proteins have yet to be identified.

In flies, TADs are formed by boundary:boundary pairing. The first evidence of physical pairing came from experiments showing that when either the Bithorax (BX-C) boundary *Mcp* or the *gypsy* transposon *su(Hw)* boundary are included in transgenes, they can induce long-distance regulatory interactions (PcG-dependent silencing and enhancer activation) between transgene inserts located many megabases (Mb) apart (Vazquez et al., 1993; Sigrest and Pirrotta, 1997; Muller et al., 1998). Regulatory interactions were even observed for transgenes inserted on different chromosomes. Subsequent *in vivo* imaging studies showed that 2, 3, and even 4 copies of these distant transgenes co-localize in imaginal disc cells (Vazquez et al., 2006; Li et al., 2011). The parameters governing boundary pairing interactions have been defined using boundary bypass, transvection and boundary competition assays (Cai and Shen, 2001; Muravyova et al., 2001; Gohl et al., 2011; Li et al., 2018). Though boundary elements can engage in promiscuous pairing interactions, there are clear partner preferences. For example, in boundary bypass assays using boundaries from the *Abd-B* region of BX-C, Kyrchanova et al. (2011) found that *Mcp* can pair with *Fab-8* but not with *Fab-7*. The other key feature is orientation dependence (Kyrchanova et al., 2008a). With few exceptions, pairing interactions are orientation-dependent. Orientation dependence can differ depending upon whether boundaries are pairing with themselves or with other boundaries. The self-pairing interactions that have been examined in detail are head-to-head (Kyrchanova et al., 2008a; Kyrchanova et al., 2008b; Fujioka et al., 2016). Self-pairing interactions take place in *trans*, and these interactions are likely responsible for the alignment and pairing of sister chromosomes and homologs (Fujioka et al., 2016; Alhai Abed et al., 2019; Viets et al., 2019; Child et al., 2021). That these interactions are head-to-head is not surprising, as head-to-tail self-pairing would generate unpaired loops and potentially disrupt transvection (Fujioka et al., 2016). Heterologous pairing interactions typically take place in *cis*, and unlike self-pairing, can be either head-to-head or head-to-tail. The former generates a TAD with a circle-loop topology while the latter generates a TAD with a stem-loop topology (Kyrchanova et al., 2008a; Fujioka et al., 2016; Li et al., 2018; Bing et al., 2024; Ke et al., 2024).

Thus far, three different mechanisms are thought to be involved in boundary:boundary pairing interactions. Probably the most common mechanism in flies is based on shared binding

sites for architectural proteins that can form dimers or multimers (Bonchuk et al. 2021; Fedotova et al. 2017). Most of the factors implicated in fly boundary function form such dimers or higher order multimers. A second mechanism for physically linking two boundaries is protein:protein interaction between heterologous DNA binding factors (Blanton et al. 2003). Yet a third mechanism would be proteins that function to bridge DNA binding proteins that are associated with each boundary. Several proteins that can potentially function as "linkers" have been identified. Included in this group are two proteins, CP190 and the 67.1 isoform of Mod(mdg4), which interact with the polydactyl zinc finger protein Su(Hw) (Harrison et al.,1993; Kim et al., 1996; Pai et al., 2004; Golovnin et al., 2007; Vogelmann et al., 2014; Melnikova et al., 2017; Melnikova et al., 2018; Melnikova et al., 2019; Kaushal et al., 2022; Golovnin et al., 2023). CP190 and Mod(mdg4) family proteins, including the 67.1 isoform, have BTB domains that assemble into dimers (CP190) or multimers (Mod(mdg4)), and thus could form a bridge linking Su(Hw) proteins bound to sites in different boundaries.

In the studies reported here, we have tested the role of the chromosomal architectural protein Su(Hw) in generating direct physical interactions between boundary elements. As a model system for this analysis we used the two boundaries, *nhomie* and *homie*, that are responsible for the formation of the ~16 kb TAD that encompasses the *Drosophila even-skipped* (*eve*) gene (Fujioka et al., 2009; Fujioka et al., 2016; Ke et al., 2024). Previous studies showed that *nhomie* and *homie* pair with themselves head-to-head, while they pair with each other head-to-tail (Fujioka et al., 2016). Like the *Mcp* and *su(Hw)* boundaries, *nhomie* and *homie* are also able to mediate long-distance regulatory interactions. We have taken advantage of this long-distance activity to probe the pairing interactions of the two *eve* boundaries. In one experimental paradigm, we used an attP site located over a dozen TADs upstream from *eve* (at -142 kb, in the 1st exon of the *hebe* gene) to insert a transgene containing two reporters driven by *eve* promoters, *eve-lacZ* and *eve-gfp* (see Figure 1). When *nhomie* or *homie* is inserted between the two reporters, one of the two reporters is activated more strongly by *eve* enhancers than the other. Activation depends on the 5'→3' orientation of the boundary relative to the two reporters in the transgene, but not on the orientation of the transgene in the chromosome. Thus, *eve-lacZ* is preferentially activated when it is positioned "downstream" of *nhomie* or "upstream" of *homie*. The same relationship holds for *eve-gfp*. We also found that the ability of a minimal 271 bp *homie* fragment (DEF) to mediate *eve* enhancer-dependent reporter activation in the -142 kb

assay depends on a predicted Su(Hw) binding site located in the D element (Fujioka et al., 2025). Since *nhomie* also has a predicted Su(Hw) binding site, this shared DNA recognition sequence could serve two functions: namely *nhomie* and *homie* self-pairing and heterologous pairing. In the studies reported here we have tested this idea. We have also analyzed interactions between the *gypsy* transposon *su*(*hw*) insulator and the two *eve* boundaries.

Results

nhomie-dependent reporter activation

To assay the long-distance pairing activity of the *nhomie* boundary, we inserted a "minimal" (602 bp) version of *nhomie* into the dual reporter in each orientation. The resulting transgenes were then integrated into the -142 kb *attP* site to give four different transgene configurations: *G-nhomie-L* and *G-eimohn-L* (Figure 1 and Figure 1-figure supplemental 1), and *L-nhomie-G* and *L-eimohn-G* (Figure 1-figure supplemental 2). In the transgenes *G-nhomie-L* and *G-eimohn-L* (diagrammed in Figure 1A), the *lacZ* reporter is located between the transgene *nhomie* and the *eve* TAD. Conversely, in the transgenes *L-nhomie-G* and *L-eimohn-G* (shown in Figure 1-figure supplemental 2), the *gfp* reporter is located between the transgene *nhomie* and the *eve* TAD. Upstream of the *attP* insertion site are enhancers for the *hebe* gene, which are active in stage 12-16 embryos (Fujioka et a., 2025). Shown in Figure 1 is a negative control transgene containing phage *lambda* DNA sequences (*G-lambda-L*) instead of *nhomie*. It is oriented so that *lacZ* is on the *eve* side of the *lambda* DNA, while *gfp* is on the same side as the *hebe* enhancers.

In the transgene *G-nhomie-L* (shown in Figure 1B), *nhomie* is oriented so that *lacZ* is on the *eve* side of *nhomie*, which is in the "downstream" position. In this configuration, *lacZ* (but not *gfp*) is preferentially activated by the *eve* enhancers (Fujioka et al., 2016). At the blastoderm stage, the *eve* stripe enhancers drive *lacZ* expression (Fig 1B and Figure 1-figure supplemental 1A), while in stage 13 embryos, *lacZ* expression is driven by the *eve* neurogenic, mesodermal, and anal plate ring (APR) enhancers (Figure 1C and Figure 1-figure supplemental 1A). Quantification of *lacZ* and *gfp* expression in the APR confirmed the preferential expression of *lacZ* (Figure 1D, *G-nhomie-L*). Activation of the *lacZ* reporter by the *eve* enhancers depends upon the presence of *nhomie*, as the *lacZ* reporter is not activated by the *eve* enhancers in the

lambda DNA control at either stage (Figure 1B and C). Reporter activation also depends upon the orientation of *nhomie* in the transgene. As shown in Figure 1B and C (also see Figure 1-figure supplemental 1A), the *eve* enhancers drive very little *gfp* expression from the *G-nhomie-L* transgene. However, since the *gfp* reporter is on the same side of the *nhomie* as the *hebe* enhancers, it is activated by *hebe* enhancers in stage 13 embryos. The *gfp* reporter is also activated by the *hebe* enhancers in the *lambda* DNA control (Figure 1A); however, the control differs from *G-nhomie-L* in that the *lacZ* reporter is not insulated from the *hebe* enhancer, and they also activate its expression. In *G-eimohn-L*, where *nhomie* is inverted, the *gfp* reporter is in the "downstream" position (on the *eve* side) relative to the boundary. In this configuration the *gfp* reporter is activated by the *eve* stripe enhancers at the blastoderm stage (Figure 1B and Figure 1-figure supplemental 1B), and by the tissue-specific enhancers in stage 13 embryos (Figure 1C and Figure 1-figure supplemental 1B). It also activated by the *hebe* enhancers, while the *lacZ* reporter is not. Quantification of *lacZ* and *gfp* expression in the APR confirmed this preferential expression of *gfp* rather than *lacZ* (Figure 1D, *G-eimohn-L*).

An analogous set of results is observed for the two transgenes *L-nhomie-G* and *L-eimohn-G*, in which *gfp* is on the *eve* side of the *nhomie*, and *lacZ* is on the *hebe* enhancer side. For *L-nhomie-G*, the *eve* enhancers activate *gfp* while *lacZ* is regulated by the *hebe* enhancer, since *gfp* is in the "downstream" position (Figure 1-figure supplemental 2A). When the orientation of *nhomie* is flipped to give *L-eimohn-G* (*lacZ* is now in the "downstream" position), *lacZ* is preferentially activated by both the *eve* and *hebe* enhancers, while *gfp* is not (Figure 1-figure supplemental 2B).

While orientation-dependent pairing of the transgene *nhomie* with the endogenous *nhomie* and *homie* boundaries results in the preferential activation of the "downstream" reporter, the close physical proximity of the reporter on the "upstream" side of the transgene *nhomie* to the enhancers in the *eve* TAD can also trigger its activation. Activation of the upstream reporter is relatively weak (see Figure 1) and is best visualized when *lacZ* is upstream of the transgene *nhomie*, and the digoxigenin procedure is used for *in situ* hybridization. This is shown for the *G-nhomie-L* and *G-eimohn-L* pair in Figure 1-figure supplemental 1. As was observed with HCR-FISH probes, only *lacZ* transcripts are detected in *G-nhomie-L* embryos using digoxigenin *in situ* hybridization. However, when *gfp* is downstream of the transgene *nhomie* in *G-eimohn-L* and should be activated by the *eve* enhancers, we detect not only *gfp* but also *lacZ* transcripts. The

lacZ probe in the digoxigenin experiment is ~2.5x longer than the *gfp* probe, and this difference may explain why *lacZ* transcripts are observed in *G-eimohn-L* embryos. Similar results are obtained for the second pair of *nhomie* inserts (*L-nhomie-G* and *L-eimohn-G*): when *gfp* is downstream of the transgene *nhomie*, a low level of *lacZ* transcripts is detected (Figure 1-figure supplemental 2).

Physical interactions between the reporters at -142 kb and the eve TAD

We used MicroC to probe the physical interactions between the *nhomie* transgenes at -142 kb and sequences in the *eve* TAD. Figure 2A shows the MicroC contact profile in the chromosomal segment between the *eve* TAD and the *attP* site in the 1st exon of the *hebe* gene, as well as a blowup of both the *eve* TAD and the insertion site. Note that there are multiple TADs in the 142 kb chromosomal segment between *eve* and the insertion site at the beginning of the *hebe* gene. As reported previously for the *lambda* DNA control (Bing et al. 2024), weak physical interactions can be detected in 12-16 hr embryos collected at 25^{o}C (Figure 2B and 2C) even though we do not observe activation of either reporter by the *eve* enhancers (Figure 1A). We suspect that the weak contacts seen for the *lambda* control may be mediated by the two *eve* promoters in the transgene.

A different result is observed for the two *nhomie*-containing transgenes, *G-nhomie-L* and *G-eimohn-L*. In both cases, the physical interactions in 14-16 hr embryos recapitulate the pattern of activity of the transgene reporters. For *G-nhomie-L,* the *lacZ* reporter preferentially interacts with sequences in the *eve* TAD. This interaction between the transgene and *eve* is shown in Figure 2D and E. As can be seen in the blow-up, the frequency of crosslinking events between *lacZ* and sequences in the *eve* TAD is much higher than those between *gfp* and the *eve* TAD.

While the *lacZ* reporter preferentially interacts with sequences in the *eve* TAD, contacts between the *gfp* reporter and the *eve* TAD are much more frequent than those observed for either reporter in the *lambda* control (compare Figure 2B and C with Figure 2D and E). This difference is likely due to the fact that *nhomie* interactions with *eve nhomie* and *homie* brings the *gfp* reporter into sufficiently close proximity for it to interact with sequences in the *eve* TAD, even though the pairing orientation of *nhomie* with the *eve* boundaries favors interactions with *lacZ.*

When *nhomie* is inverted in the transgene to give *G-eimohn-L*, the pattern of physical interactions between the reporters and sequences in the *eve* TAD is the opposite of that observed

for *G-nhomie-L*. The primary interactions are between the *gfp* reporter and the *eve* TAD while the secondary interactions are between *lacZ* and the *eve* TAD (Figure 2F and G). This can be seen by comparing the blowups for Figure 2E and 2G.

The different topology of the loops generated when the *nhomie* elements in *G-nhomie-L* and *G-eimohn-L* interact with *nhomie* and *homie* in the *eve* TAD results in other differences in the contact patterns. For example, in the *G-nhomie-L* insert, *gfp* comes into contact with the TADs immediately upstream (blue arrowhead in Figure 2E) and downstream (green arrowhead) of the *eve* TAD. When the orientation of *nhomie* is flipped so that the *gfp* reporter is activated instead of *lacZ*, the interaction pattern with neighboring sequences changes. In this case, it is *lacZ* that interacts with sequences in the TADs upstream (blue arrowhead in Figure 2G) and downstream (green arrowhead) of the *eve* TAD.

Viewpoints from the lacZ and gfp reporters

To further document that boundary orientation in the transgene determines which of the two reporters preferentially interacts with the *eve* TAD, we generated "virtual 4C" viewpoints of the Micro-C data specifically focused at the reporters and quantified the amount of contact with *eve*. In this analysis, Micro-C contact pairs are restricted to those that involve a specific region of interest, i.e. the *gfp* reporter (Figure 3A) or *lacZ* reporter (Figure 3B) in the data with the *G-nhomie-L* insert, and the *gfp* and *lacZ* reporters for the *G-eimohn-L* insert (Figures 3C, D). These "virtual 4C" data can also be visualized as 1-dimensional read coverage tracks. Average contact counts between the reporters and the *eve* locus are shown in Figure 3E. For the *G-nhomie-L* insert, the *lacZ* reporter interacts strongly with sequences within the *eve* TAD, while there is little interaction with sequences in TADs located beyond either the *nhomie* or *homie* boundaries. While the *gfp* reporter also interacts with sequences in the *eve* TAD, the interactions are highest near the boundaries, and lower within the *eve* TAD. Additionally, the *gfp* reporter contacts sequences in the TADs flanking the *eve* gene. A similar pattern is observed for *G-eimohn-L*, except in this case, *gfp* preferentially interacts with the *eve* TAD, and the *lacZ* reporter contacts areas flanking the *eve* TAD. The different topologies of the loops generated by interaction between *nhomie* in *G-nhomie-L* and *G-eimohn-L* and *nhomie* / *homie* in the *eve* TAD are shown in Figure 3F.

The Su(Hw) site in nhomie is required for long-distance regulatory interactions

Fujioka et al. (2025) showed that the predicted Su(Hw) binding site in a minimal 271 bp *homie* boundary (called DEF) is required for mediating long-distance regulatory interactions in the -142 kb assay. Since *nhomie* also has a predicted Su(Hw) binding site, we tested whether mutations in this site impact regulatory interactions in the -142 kb assay. Figure 4A and B show the control *G-nhomie-L* and the corresponding Su(Hw) binding site mutant transgene, *G-nhomieΔSH-L*. As evident from a comparison of wild-type and Su(Hw) mutant embryos, expression of the *lacZ* reporter both at the blastoderm stage and later in development is largely lost when the *nhomie* Su(Hw) binding site is mutated. Quantification of *lacZ* and *gfp* confirmed the staining results (Figure 4C).

As the digoxigenin *in situ* hybridization procedure can be used to amplify weaker *lacZ* signals, we also used it to assay the effects of mutating the *nhomie* Su(Hw) binding sites, and this is shown in Figure 5A and B. While little if any *lacZ* expression was detected using HCR-FISH, *lacZ* transcripts driven by the *eve* enhancers can be detected in blastoderm and early gastrula *G-nhomieΔSH-L* embryos using digoxigenin *in situ*. The number of *lacZ*-positive cells is, however, substantially reduced compared to WT *nhomie*. Interestingly, in older germband extended and germband retracted embryos, *eve* enhancer-dependent expression in the APR and the CNS is largely absent. The loss of the Su(Hw) binding site also impacts the blocking ability of *nhomie*, since *lacZ* expression driven by the *hebe* enhancers in midline cell clusters is now observed (Figure 5B, stage 13, “13” and “13v”).

The Su(Hw) site in homieCDEF is required for long-distance regulatory interactions

We also reexamined the effects of Su(Hw) binding site mutation in *homie* on long-distance regulatory interactions. Instead of the minimal 271 bp DEF *homie* element used in our previous study (Fujioka et al., 2025), we used a larger 367 bp *homie* element, CDEF. Like *nhomie*, the relative orientation of the *homie* in the transgene determines which of the two reporters is preferentially activated by the *eve* enhancers. For these experiments we oriented the wild-type *homie* and the Su(Hw) mutant *homieΔSH* in the transgene so that *lacZ* was located “upstream” (Figure 5C and D, and Figure 6; *G-eimoh-L* and *G-eimoh-ΔSu(Hw)-L*). In this configuration, the *lacZ* reporter is activated by the *eve* enhancers when the transgene *homie* pairs with the *eve*

boundaries. The transgene was then inserted into the -142 kb attP site so that the *lacZ* reporter is located on the *eve* side of the transgene *homie*.

Figure 6 shows *G-eimohΔSH-L* HRC-FISH *in situs*, while Figure 5C and D shows digoxigenin *in situs*. Little or no *eve*-enhancer-dependent *lacZ* expression can be detected in *G-eimohΔSH-L* in stage 5 (or 7) embryos using either *in situ* hybridization procedure. Thus, the loss of the Su(Hw) binding site appears to have even greater impact on *homie*-dependent regulatory interactions at this stage in development than observed for *nhomie* (compare Figure 5B and D). On the other hand, in stage 11 and 13 embryos in *G-eimohΔSu(Hw)-L*, weak *lacZ* expression can be detected in the APR, but not in *G-nhomieΔSu(Hw)-L*. Quantification of *lacZ* and *gfp* expression in the APR confirmed the staining results (Figure 6C). For both cases, several midline cell clusters in the CNS were observed, indicating that in addition to being largely unable to mediate long-distance regulatory interactions, the Δ*SH* mutants are unable to fully block the *hebe* enhancers from activating *lacZ* expression (Figure 4B, 5B, 5D and 6B).

Mutation of Su(Hw) binding sites in nhomie and homieCDEF disrupts long-distance physical interactions.

To better understand how the loss of the Su(Hw) binding sites in *nhomie* and *homie* impacts the ability of these TAD boundaries to mediate long-distance regulatory interactions, we used MicroC to probe the physical interactions between the transgenes and the *eve* TAD. The MicroC contact maps for *G-nhomie-L* and *G-nhomieΔSH-L* are shown in Figure 7A and B, while Figure 7C and D show "virtual 4C" viewpoints from the transgene *lacZ* and *gfp* reporters (similar to the analysis in Figure 3). As expected from the substantial reduction in reporter activity, contacts between the *lacZ* reporter in *G-nhomieΔSH-L* and sequences in the *eve* TAD are diminished. This change can be seen in the blow-ups in panels 7A and B and in the *lacZ* and *gfp* viewpoints in panels C and D. Quantitation indicates that there is a nearly 10-fold reduction in contact frequency (Figure 7E). Interestingly, however, the pattern of physical interactions between *G-nhomieΔSH-L* and the surrounding TADs, with *eve* and the TADs surrounding *eve* appear to be quite similar to that of the wild-type *G-nhomie-L* insert (Figure 7-figure supplemental 1). This would suggest that the transgene boundary still pairs in the same orientation-dependent manner with the endogenous *eve* locus, just less frequently or less stably than it does when the Su(Hw) site is intact**.**

The MicroC contact profile for the *G-eimoh-L* and *GeimohΔSH-L* inserts are shown in Figure 8A and B. As was the case for the *G-nhomieΔSH-L* insertion, there is a substantial reduction in the physical interactions between the *G-eimohΔSH-L* and sequences in the *eve* TAD. This can be seen by comparing the *lacZ* and *gfp* reporter "virtual 4C" viewpoints for *G-eimoh-L* in Figure 8C with those for *G-eimohΔSH-L* in Figure 8D. Although the frequency of physical interactions is greatly reduced (Figure 8E), the residual pattern of interactions between *G-eimohΔSH-L* and the surrounding TADs with *eve* and the TADs surrounding *eve* still resemble that seen for *G-eimoh-L*.

Since mutating the Su(Hw) binding sites in both *nhomie* and *homie* results in the activation of the *lacZ* reporter by the *hebe* enhancers located just beyond the *gfp* reporter, we calculated the "insulation" score. We used Fan-C and a window of 4 kb to analyze cross-TAD contacts for *lambda* DNA, the wild-type and Su(Hw) mutant *nhomie* and *homie* boundaries (see Methods). For this purpose, we measured the contact frequency between sequences immediately upstream and downstream of the transgene insertions. Figure 7F shows the insulation score for wild -type and Su(Hw)-mutant *nhomie* relative to that of *lambda*, while Figure 8F shows the insulation score for wild-type and Su(Hw)-mutant *homie* relative to that of *lambda*. In both cases, there is a significant drop due to the Su(Hw) binding site mutation.

Long-distance physical interactions between the transgene boundary and the endogenous nhomie and homie

The regulatory interactions between the reporters in the transgene insert and the *eve* enhancers depend upon the physical pairing of the transgene boundary with the endogenous *nhomie* and *homie*. In previous experiments (Bing et al., 2024), we found that when the viewpoint is centered on *homie* in the transgene rather than one of the reporters, the interactions with *eve* peak at the *nhomie* and *homie* boundaries (Figure 9C). This is also true for transgenes containing the *nhomie* boundary. Figure 9A shows that the interactions between *nhomie* in the *G-nhomie-L* transgene and *eve* are centered on the *nhomie* and *homie* boundaries. These findings support the conclusion that pairing of the transgene boundary with the two *eve* boundaries is directly responsible for physically linking the transgene to the *eve* TAD.

As would be predicted by the boundary pairing model, mutations in the Su(Hw) binding site result in a disruption of the physical interactions between the transgene boundary and *nhomie* and *homie* in the *eve* locus. For the Su(Hw) mutation in *G-nhomieΔSH-L*, the physical interactions between the transgene boundary and the two *eve* boundaries are substantially reduced (Figure 9B). Moreover, consistent with the idea that the shared Su(Hw) binding sites are important for *nhomie* self-pairing and for heterologous pairing with *homie*, the prominent peaks for *nhomie*-transgene with both *nhomie* and *homie* are substantially reduced in the *nhomieΔSH* viewpoint (Figure 9B). The physical interactions are not completely lost, as there are still small peaks that map to both *nhomie* and *homie*.

The physical contacts between the transgene *homieΔSH* and the two *eve* boundaries are also compromised by the Su(Hw) binding site mutation (Figure 9C and D). Moreover, as was the case for *nhomie*, *homie* self-pairing (*homie*-transgene with *homie*) and heterologous pairing (*homie*-transgene with *nhomie*) largely depend upon the shared Su(Hw) binding sites.

Su(Hw) mutant *homie* retains pairing activity in transvection assays

While the Su(Hw) mutations disrupt long-distance interactions between the transgene boundary and the boundaries in the *eve* TAD, weak physical interactions can still be detected in viewpoints from the reporters and the transgene boundary. This would suggest that factors other than Su(Hw) must be involved in pairing interactions, and that they might be sufficient on their own to mediate physical interactions in less demanding assays.

To test this possibility, we used a transvection assay in which a *lacZ* reporter transgene interacts with a transgene containing enhancers, each inserted into an *attP* site distant from *eve*, where long-range interactions with the endogenous *eve* enhancers are not observed (Fujioka et al., 2016). As pairing interactions in *trans* in this *attP* environment are relatively few, the reporter is only weakly activated by the *eve* enhancers when the *lacZ* reporter carries *lambda* DNA and the enhancer transgene carries the *homieCDEF* that was used in -142kb assay (Figure 10A). In contrast, when both transgenes have the *homieCDEF* inserted in the *same* orientation relative to the reporter and the enhancers, the *lacZ* reporter is activated strongly by the *eve* mesodermal and APR enhancers (Figure 10B). *Trans*-activation is also observed when the 367 bp *homie* fragment CDEF is paired with the smaller 271 bp *homie* fragment DEF (Figure 10C). In contrast to the -142 kb assay, the regulatory interactions in the transvection assay are less

sensitive to mutations in the Su(Hw) binding site. While mutation of the Su(Hw) site in DEF (DΔSuEF, located in the reporter transgene) weakens regulatory interactions, the *eve* enhancers are still able to active *lacZ* expression more strongly than with *lambda* DNA (Figure 10D relative to 10A). We performed a similar set of transvection experiments with a 200 bp *nhomie* fragment. Mutations in the Su(Hw) site in this fragment also weakened but did not eliminate stimulation by the *eve* enhancers.

Shared Su(Hw) binding sites promote pairing interactions in the transvection assay

In previous studies (Fujioka et al. 2025), we found that the *gypsy* insulator is unable to mediate regulatory interactions between transgenes inserted at -142 kb and the *eve* enhancers (Figure 11-figure supplemental 1B). One interpretation of this finding is that the two Su(Hw) proteins associated with *homie* and *nhomie* are not sufficient for physical interactions with the *gypsy* insulator even though it is expected to be bound by multiple Su(Hw) proteins. An alternative possibility is that while there are interactions between the *gypsy* insulator at -142 kb and the *homie* and *nhomie* boundaries via the shared Su(Hw) proteins, these interactions are too transient for the *eve* enhancers to successfully activate reporter expression.

To distinguish between these possibilities, we used the less demanding transvection assay to test whether the single Su(Hw) binding site in *homie* is sufficient to mediate regulatory interactions with the *gypsy* insulator. Figure 11 shows that the interactions between *homie* and the *gypsy* insulator in this transvection assay are not altogether different from when *homie* is paired with itself. Moreover, unlike *homie:homie* pairing, *gypsy:homie* pairing is orientation independent: the *eve* enhancers can active *lacZ* expression independent of the relative orientation of the *gypsy* and *homie* elements at a level only slightly lower than that observed for *homie:homie* pairing interactions. Although we did not test orientation dependence for *gypsy:nhomie* pairing, the *gypsy*-containing reporter is activated by the *eve* enhancers when the enhancer transgene has *nhomie* (Figure 11-figure supplemental 1A).

Discussion

TAD formation in the boundary:boundary pairing model depends upon physical interactions between proteins that are associated with the interacting boundary elements. In one mechanism, boundaries that share binding sites for the same DNA binding protein can be linked together if that protein can assemble into homodimers and/or homomultimers. This mechanism is used by polydactyl zinc finger proteins like CTCF, Zw5, Zipic, and Pita, by the BEN domain protein Insensitive, and DNA binding proteins like GAF, Mod(mdg4), and CP190 that have BTB domains (Fedolova et al., 2017; Bonchuck et al., 2021). Unlike these chromosomal architectural proteins, Su(Hw) is not known to form homomeric complexes; however, previous studies have shown that its chromosome architectural functions depend upon shared binding sites. This was first suggested by the studies of Sigrest and Pirrotta (1997), who showed that transgenes carrying the Su(Hw)-dependent *gypsy* insulator and a Polycomb response element from the Bithorax complex could mediate long-distance Polycomb-dependent silencing of a *white* reporter. Subsequent studies by Cai and Shen (2001) and Muravyova et al. (2001) presented additional genetic evidence for the pairing of *gyspy* insulators, and this was extended by the boundary bypass experiments of Kyrchanova et al. (2008a). In these experiments, Kyrchanova et al. showed that bypass depended on shared binding sites for chromosomal architectural proteins. When multimerized binding sites for Su(Hw), CTCF, or Zw5 were paired with themselves, bypass was observed; however, when multimerized Su(Hw) binding sites were paired with multimerized CTCF or Zw5 binding sites, there was no bypass. The Kyrchanova et al. paper also showed that self-pairing is a common property of endogenous boundaries in flies.

While the genetic experiments showing that fly boundaries utilize shared binding sites in their pairing interactions are compelling, a direct demonstration of the physical interactions that are mediated by these shared sites is lacking. In fact, there is scant evidence linking binding sites for fly chromosomal architectural proteins with the physical interactions involved in self or heterologous boundary:boundary pairing. To address this question, we have used the *eve* TAD boundaries, *nhomie* and *homie*, to test the role of shared binding sites. Genetic studies have shown that, like other fly boundaries, *nhomie* and *homie* pair with themselves head-to-head. They also pair with each other, in this case in a head-to-tail configuration. This pairing interaction generates a TAD with a stem-loop topology, which has a distinctive contact profile in MicroC experiments (Bing et al. 2024; Ke et al. 2024). When *nhomie* or *homie* is included in a

dual reporter transgene inserted in an *attP* site 142 kb from *eve*, the *eve* enhancers drive reporter expression. In previous studies on *homie*, we showed that these regulatory interactions accompany the physical pairing of the transgene boundary with both of the endogenous *eve* boundaries (Bing et al., 2024). As reported here, this is also true for *nhomie* (Figs. 2 and 3). This can be seen when the transgene *nhomie* is used as a viewpoint: it contacts both *nhomie* and *homie* in the *eve* locus. Also like *homie*, the relative orientation of *nhomie* in the transgene determines which of the two reporters is activated. Moreover, the pattern of activation is a reflection of the physical contacts that are visualized with MicroC between the two reporters and sequences in the *eve* TAD.

Mutations in the shared homie and nhomie Su(Hw) binding sites disrupt self and heterologous pairing interactions.

As would be predicted if shared sites for DNA binding proteins are important for boundary function, mutations in the *homie* and *nhomie* Su(Hw) sites largely abrogate long-distance regulation by the *eve* enhancers (Figure 4, 5, and 6). Although the effects of the Su(Hw) mutation on transcriptional activation are in both cases substantial, we are able to detect regulatory interactions using the more sensitive digoxigenin *in situ* procedure (Figure 5). For *nhomieΔSH*, we detect residual *lacZ* expression in an *eve*-like stripe pattern at the blastoderm and early gastrulate stages, while there is little if any expression evident in stage 11 and 13 embryos, when *eve* is expressed in the APR, CNS, and mesoderm. In contrast to *nhomieΔSH*, only very few *lacZ*-positive cells are visible in blastoderm and early gastrula embryos in *eimohΔSH*. Instead, we detect weak *lacZ* expression in stage 11 and 13 embryos in the APR and CNS. It is not clear why enhancer-driven *lacZ* expression for *nhomieΔSH* seems to be restricted to blastoderm and early gastrulation embryos, while for *eimohΔSH*, enhancer-dependent expression is stronger in stage 11 and 13. One possibility is that residual self-pairing of the Su(Hw) mutant boundary is stronger than pairing with the heterologous boundary. This is suggested by the proximity of the relevant enhancers to the *eve* boundary whose transgene partner carries the Su(Hw) mutation. The 7-stripe enhancer that drives *eve* expression during early gastrulation is located next to the *nhomie* boundary, and this is the time when *nhomieΔSH*-dependent *lacZ* expression is highest. Likewise, the APR and CNS enhancers are located between *eve* and *homie*, and thus would closer to the *homie* boundary. Another possibility is that

nhomie and *homie* have some different stage/tissue-specific boundary factors other than Su(Hw) that contribute to pairing, resulting in stronger pairing at later stages for *eimohΔSH* relative to *nhomieΔSH*.

The homie Su(Hw) binding site mutant retains some boundary function

Although the long-distance regulatory and physical interactions of *GeimohΔSHL* with the *eve* locus is significantly reduced, it is not completely disrupted. Consistent with the idea that the mutant retains some boundary activity, we can readily detect *lacZ* expression driven by *eve* enhancers when a minimal 271 bp *homie* element, *DΔSuEF*, carrying the Su(Hw) binding site mutation is combined with the standard 367 bp (CDEF) *homie* boundary in our transvection assay (Figure 10). The likely reason is that this is a less demanding assay, as boundaries to either side of the reporter and enhancer transgenes in the chromosome are expected to be mediating homologous pairing (via head-to-head self-pairing interactions), and this would help align boundaries in the transgene and stabilize their physical interactions. By contrast, the -142 kb assay boundary pairing takes place across multiple TADs, and, as is evident from the novel contacts that are induced, requires a substantial distortion in the native organization of the chromatin fiber in between the transgene and the *eve* TAD, as well as to either side. This would likely tend to disfavor physical interactions between the distant boundary elements.

Specificity versus promiscuity in pairing interactions

Although there are multiple TAD boundaries between the -142 kb attP site and *eve*, none have Su(Hw) binding sites, and there is no indication of pairing interactions between these boundaries and either *homie* or *nhomie* in the MicroC contact profiles and the viewpoints from the transgene towards *eve* (Figure 2, 3, 7, 8, and 9). ChIP experiments indicate that there are two Su(Hw) peaks to the left of the -142 kb attP site that could potentially interact with the transgene boundaries or the endogenous *eve* boundaries (Figure 7-figure supplemental 2). However, we did not detect any pairing interactions in the MicroC contact profiles. This would suggest that the presence of shared binding sites in the neighborhood is not in itself sufficient for cross-TAD interactions. Consistent with this idea, we found that a 451 bp *gypsy* transposon Su(Hw) element was unable to mediate regulatory interactions between a transgene reporter inserted at -142 kb and the *eve* enhancers (Fujioka et al. 2025: see Figure 11-figure supplemental 1B). On the other hand, shared Su(Hw) sites would appear to be sufficient for pairing interactions in less

demanding assays, as the *gypsy* insulator is able to support transvection when paired with *homie* (Figure 11) or *nhomie* (Figure 11-figure supplemental 1A). In both cases, the level of reporter expression is closer to that observed when *homie* or *nhomie* are paired with themselves than it is to that seen when one of the transgenes carries *lambda* DNA in place of a boundary. Thus, the observed levels of specificity versus promiscuity depend upon the design of the assays that are used to detect pairing interactions.

Mechanisms underpinning TAD assembly

Two different mechanism have been proposed to explain how TADs are formed. One is the physical pairing of neighboring boundary elements in *cis* that has been described here, while the other is the cohesin loop extrusion/CTCF road block model (Dixon et al., 2012; Rao et al., 2017; Fudenberg et al., 2017; Davidson and Peters, 2021; Dekker and Mirny, 2024). While our findings are completely compatible with the expectations of the boundary:boundary pairing model, they are not consistent with the mechanisms thought to be deployed in the loop extrusion model.

In the loop extrusion model, in order for the *eve* enhancers to activate reporters in transgenes inserted in the -142 kb attP site, the cohesin complex would have to break through multiple intervening TAD boundaries and come to a halt when it encounters the transgene *nhomie* or *homie* boundary. In this case the reporter on the *eve* side of the transgene boundary will be in the same loop domain as the *eve* enhancers. Since the loop extrusion mechanism can only generate stem-loops, preferential physical contacts with *eve* enhancers would be restricted to the reporter on the *eve* side of the transgene boundary, which conforms to the classic definition of a boundary element (Kellum and Schedl, 1992). This would be completely independent of the orientation of the boundary element (*nhomie* or *homie* in the transgene). There is no mechanism in the loop extrusion model by which the reporter on the *hebe* enhancer side of the transgene boundary could be preferentially brought into contact with the *eve* enhancers. However, this is precisely what is observed when the orientation of the transgene boundary is manipulated. When the transgene *nhomie* is in the opposite orientation from the endogenous *nhomie*, the reporter on the *hebe* side of the boundary is activated by the *eve* enhancers (Figure 1). Likewise, when the transgene *homie* is in the same orientation as the endogenous *homie*, the reporter on the *hebe* enhancer side of the transgene boundary is preferentially activated by the *eve* enhancers (Fujioka et.al. 2016).

The shortcomings of the loop extrusion model are also clearly evident in the pattern of physical contacts seen in MicroC experiments. As predicted by the boundary pairing model, physical interactions between the two reporters and sequences in the *eve* TAD track completely with relative reporter activity (Figs. 2 and 3 for *nhomie*; Figs. 8 and 9, and Bing et al. 2024 for *homie*). Moreover, independent of the orientation of the boundary in the transgene, it physically interacts with both *nhomie* and *homie* in the *eve* TAD (Figure 9 and Bing et al. 2024). This would rule out a model in which cohesin bypasses the "inappropriately" oriented *nhomie* or *homie* boundary and stops at some TAD boundary beyond the *hebe* gene so that the reporter on the "wrong side" of the boundary is in the same loop domain as the *eve* enhancers.

These are not the only shortcomings of the loop extrusion model. There is no mechanism in this model that would enable enhancers on one homolog to activate a reporter on the other homolog. However, we have shown here (Figure 10 and Figure 11-figure supplemental 1) and elsewhere (Fujioka et al., 2016) that *nhomie* and *homie* can mediate transvection either by pairing with themselves or with each other. For self-pairing, the *nhomie* or *homie* elements in the enhancer and reporter transgenes must be in the same orientation, while for heterologous pairing (*nhomie:homie*) they must be in the opposite orientation (Fujioka et al. 2016). Moreover, although they contain only a single Su(Hw) binding, both *eve* boundaries can mediate transvection with the *gyspy* insulator as a pairing partner. In the case of *gypsy:homie*, we found that this interaction is orientation independent (Figure 11). The fact that *gypsy* can function in *trans* with *nhomie* and *homie*, but cannot mediate long-distance interactions in the -142 kb assay, is also inconsistent with the loop extrusion model for the formation of TAD boundaries.

Figures

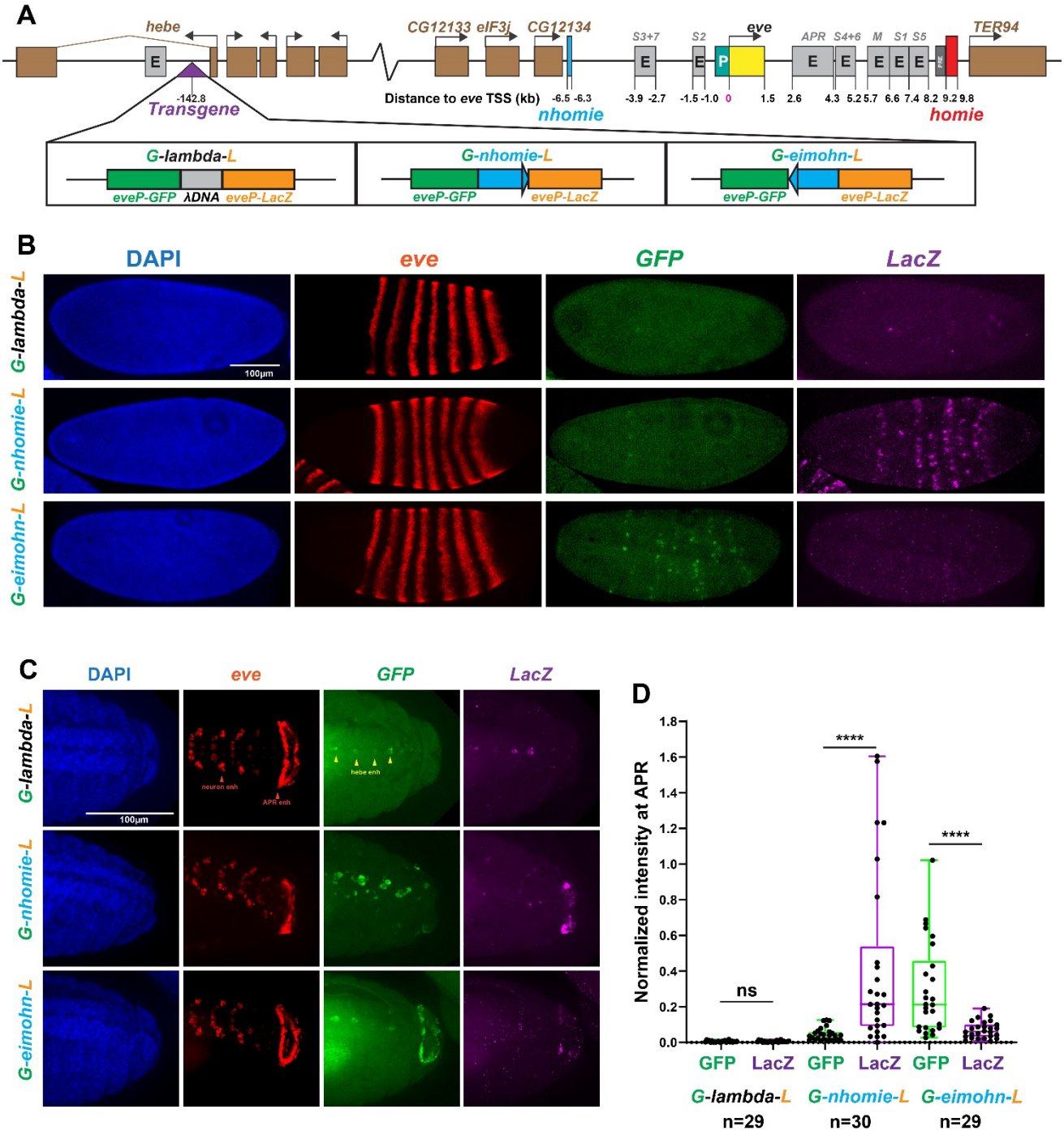

Figure 1. Activation of *nhomie* containing transgenes inserted -142 kb from *eve* by *eve* enhancers.

Figure 2

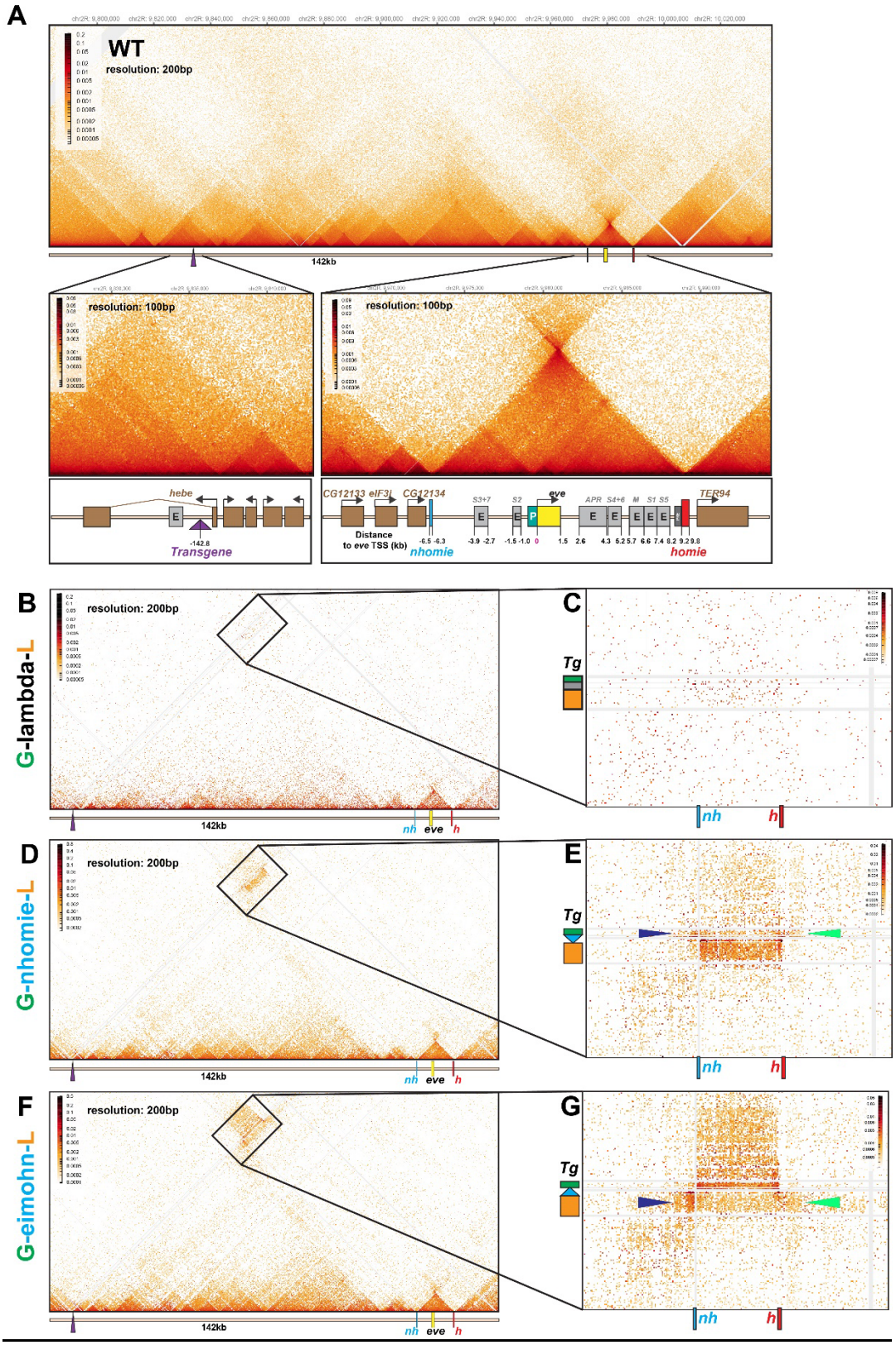

Figure 2. *nhomie* containing transgenes physically interact with the *eve* TAD.

Figure 3

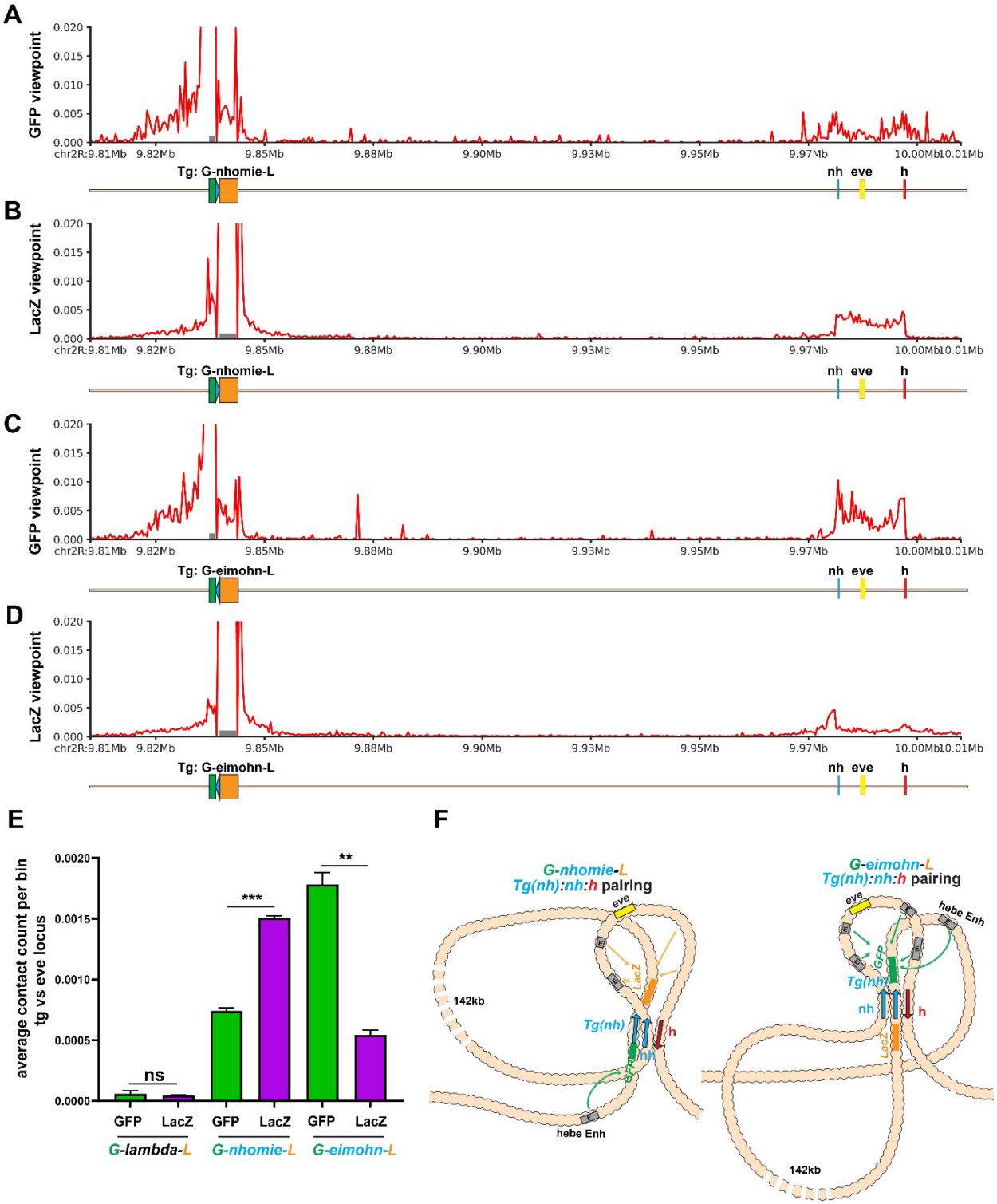

Figure 3. MicroC viewpoints from the *G-nhomie-L* and *G-eimohn-L* reporters.

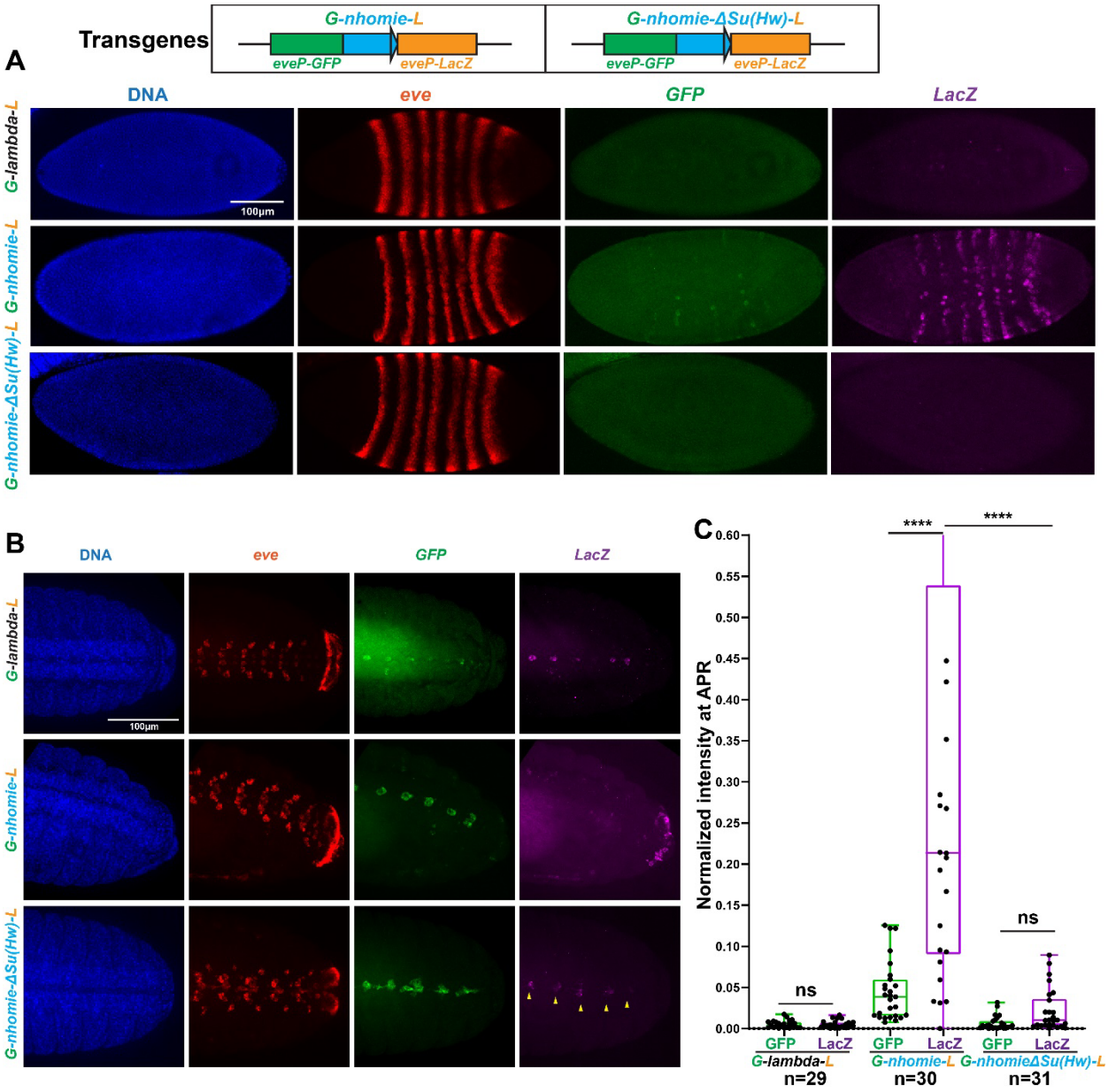

Figure 4. Mutations in *nhomie* su(Hw) binding site disrupts activation of transgene reporter expression by *eve* enhancers.

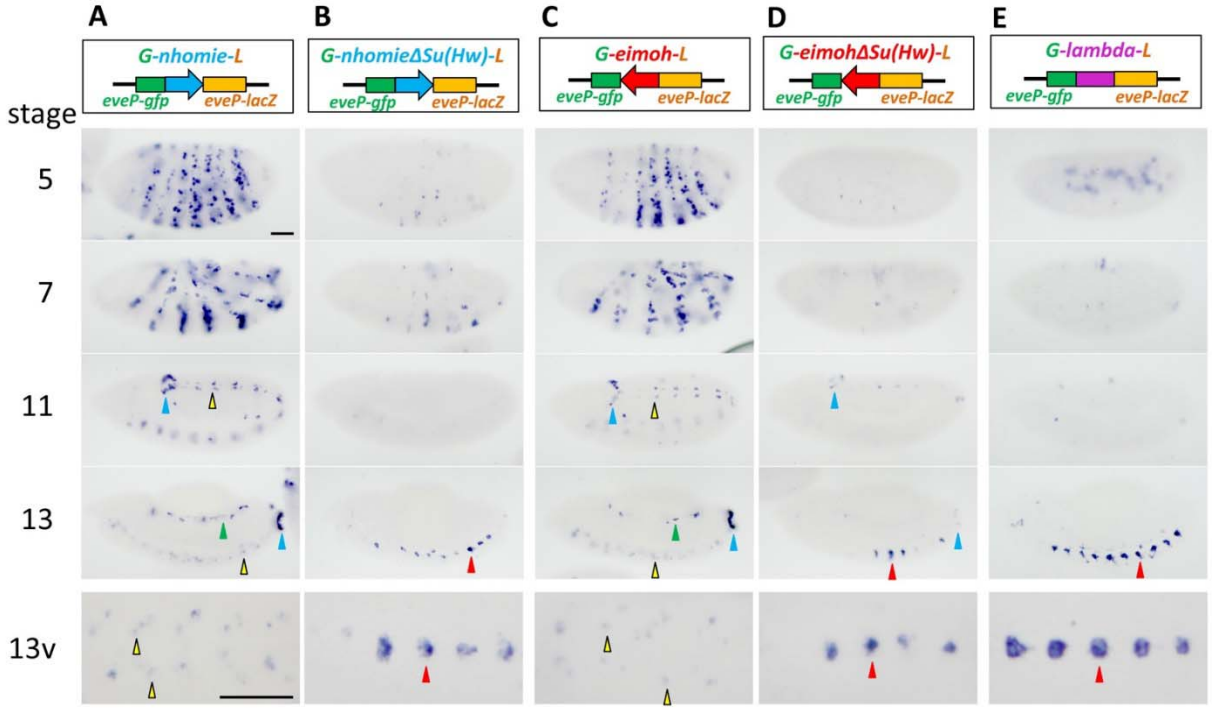

Figure 5 Digoxigenin in situs: wild type and su(Hw) mutant *nhomie* and *homie*.

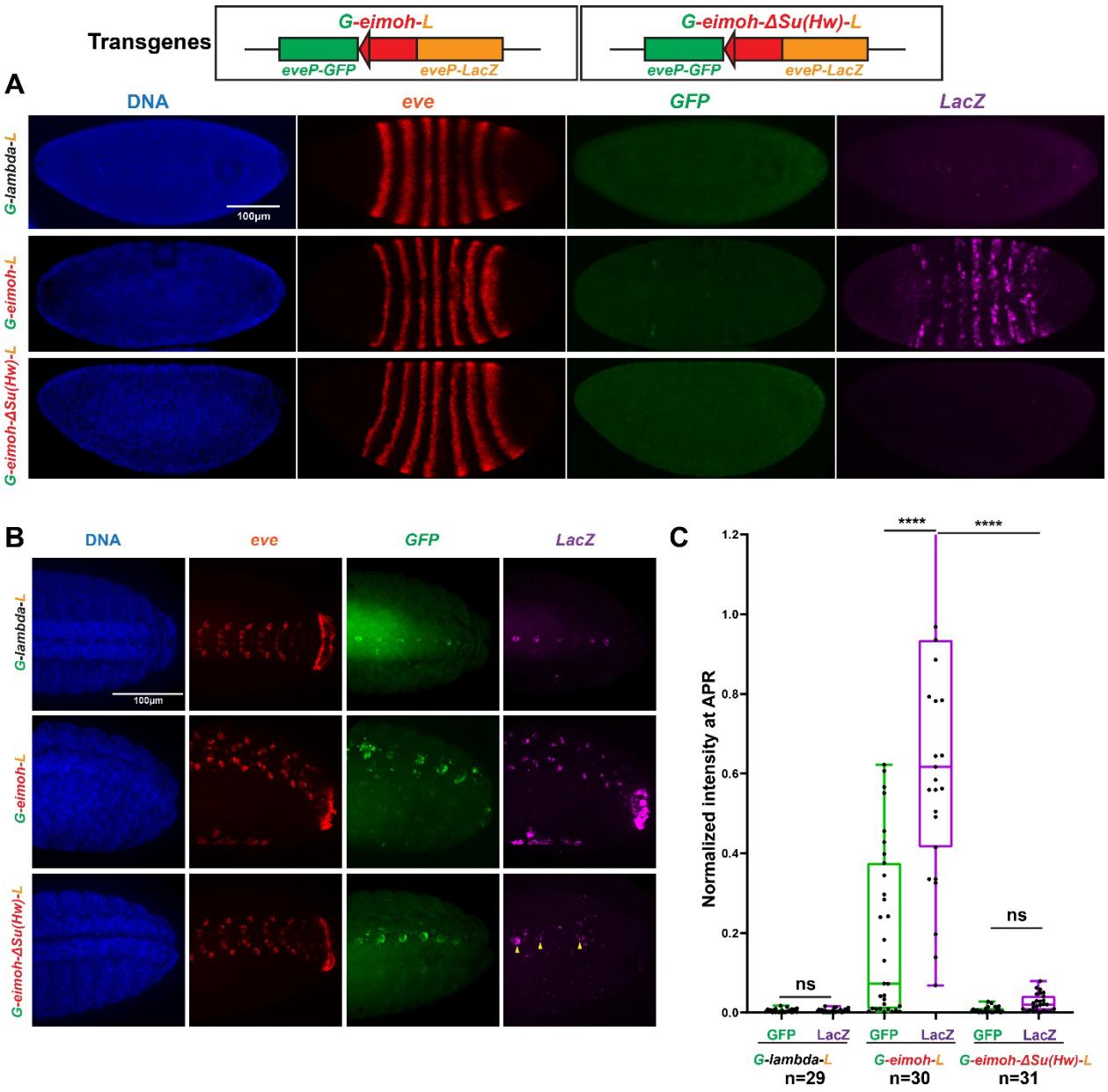

Figure 6. Mutations in *homie* su(Hw) binding site disrupts activation of transgene reporter expression by *eve* enhancers.

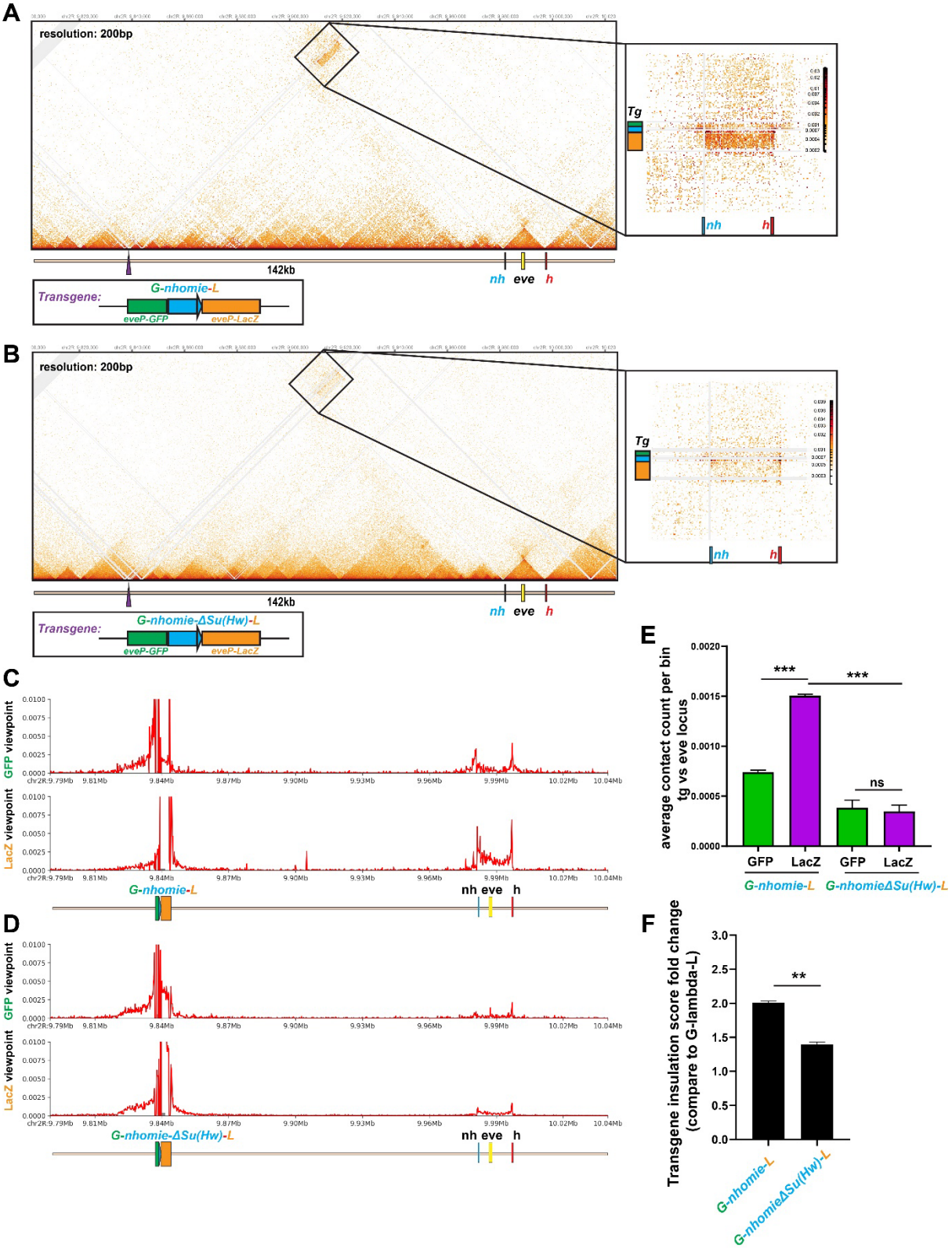

Figure 7. Mutations in *nhomie* su(Hw) binding site disrupts physical interactions between the transgene and sequences in the *eve* TAD.

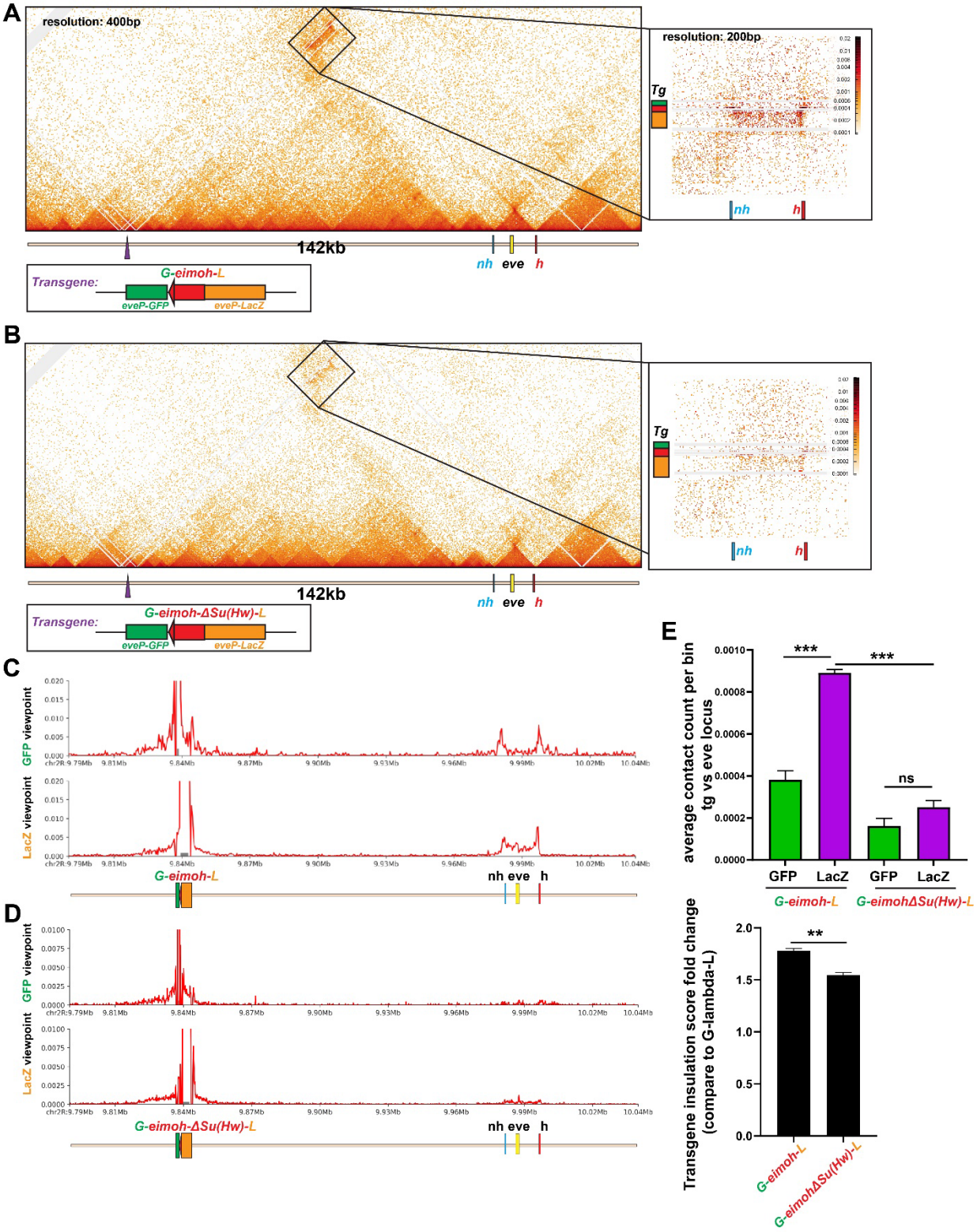

Figure 8. Mutations in *homie* su(Hw) binding site disrupts physical interactions between the transgene and sequences in the *eve* TAD.

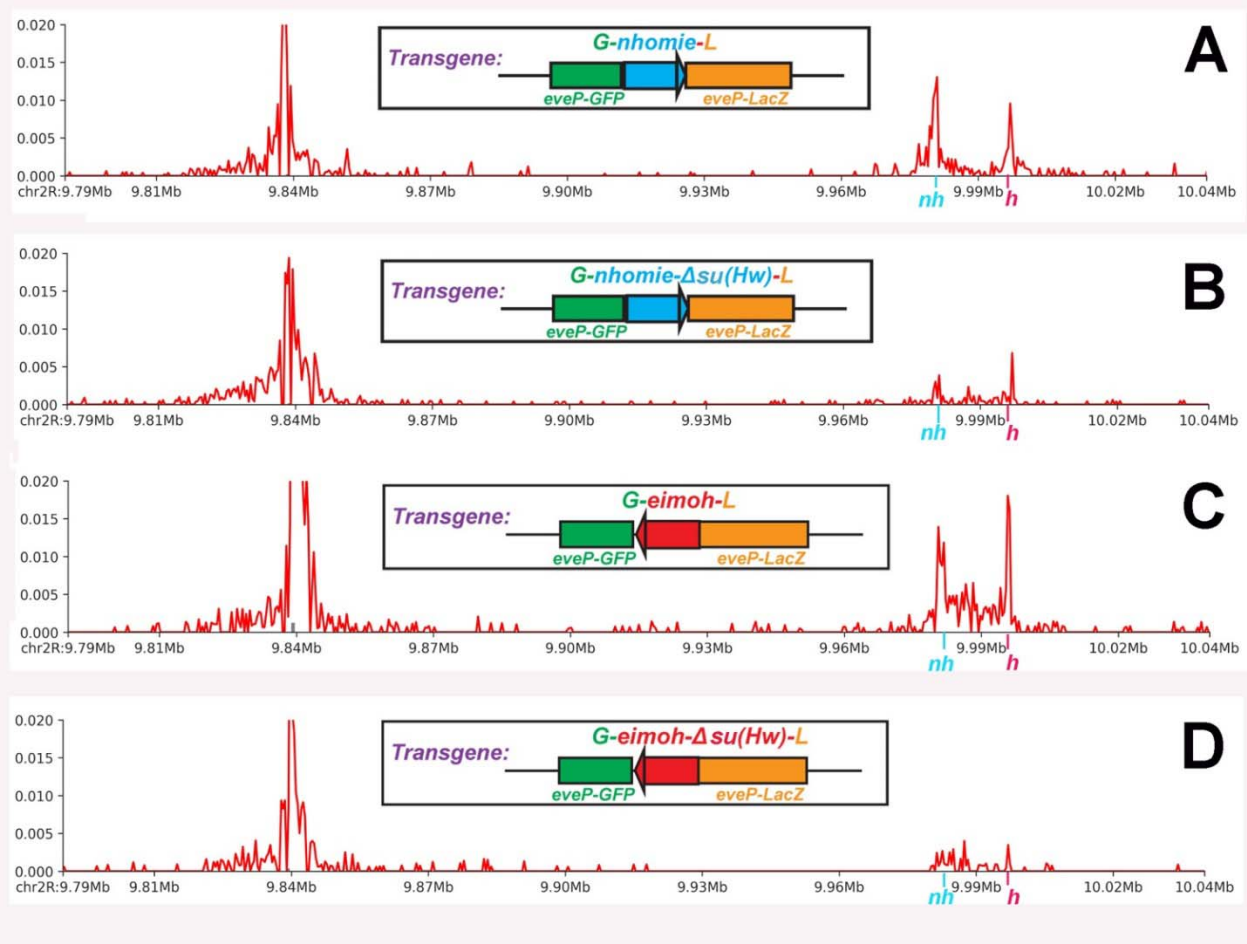

Figure 9. Viewpoints from the transgene boundaries.

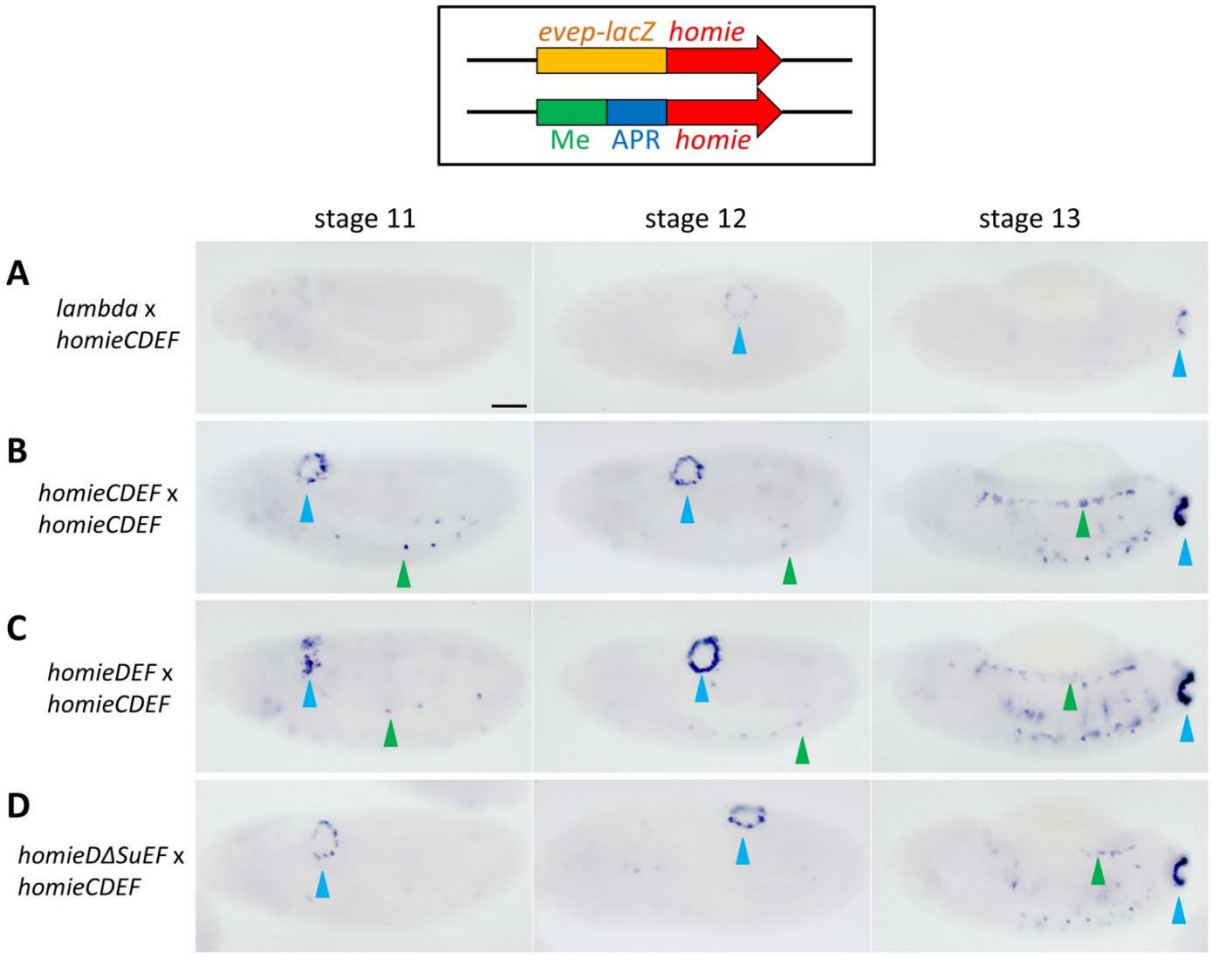

Figure 10. *homie* transvection is weakened loss of the su(Hw) binding site.

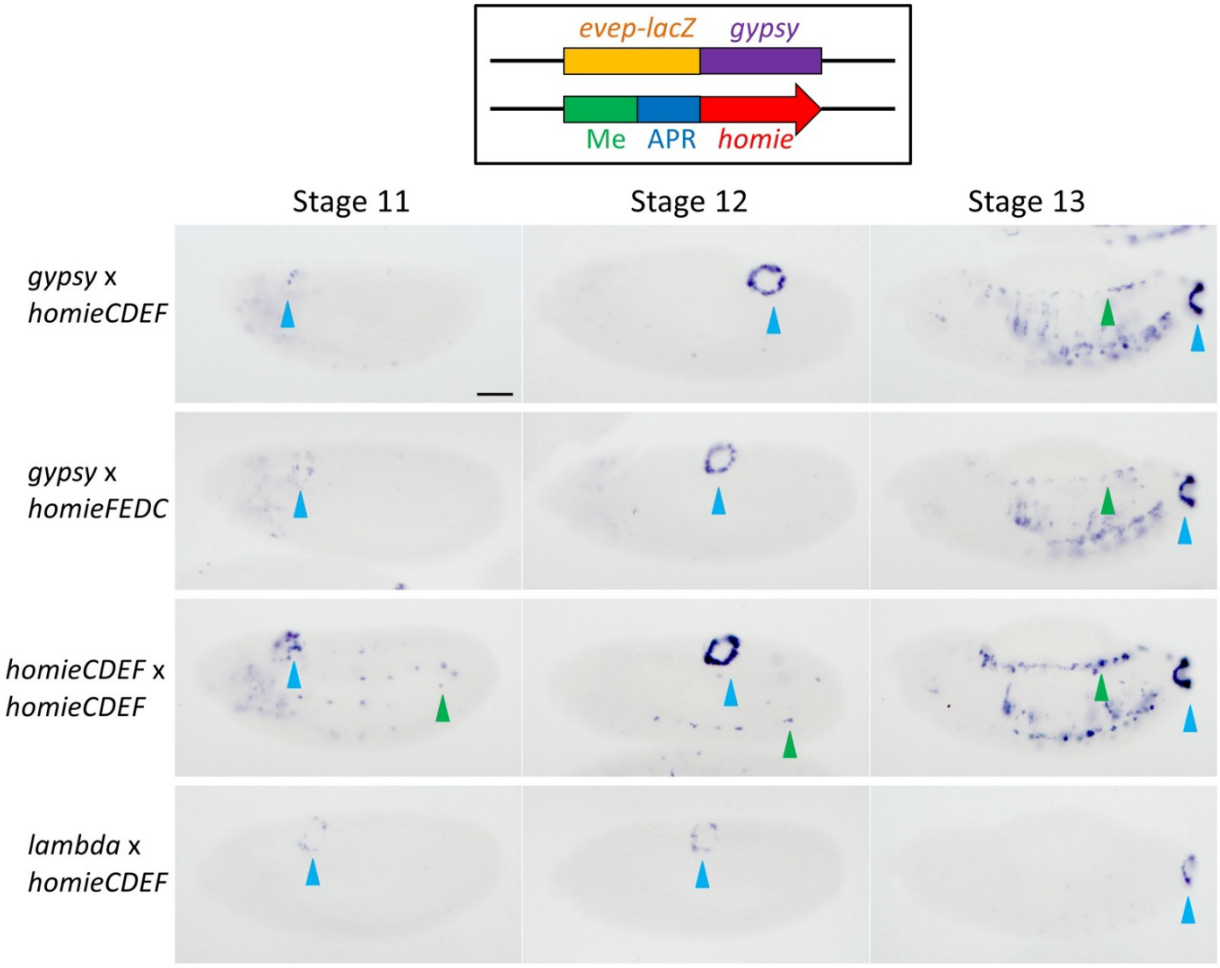

Figure 11. The su(Hw) *gypsy* insulator supports transvection with *homie*.

Figure Supplemental

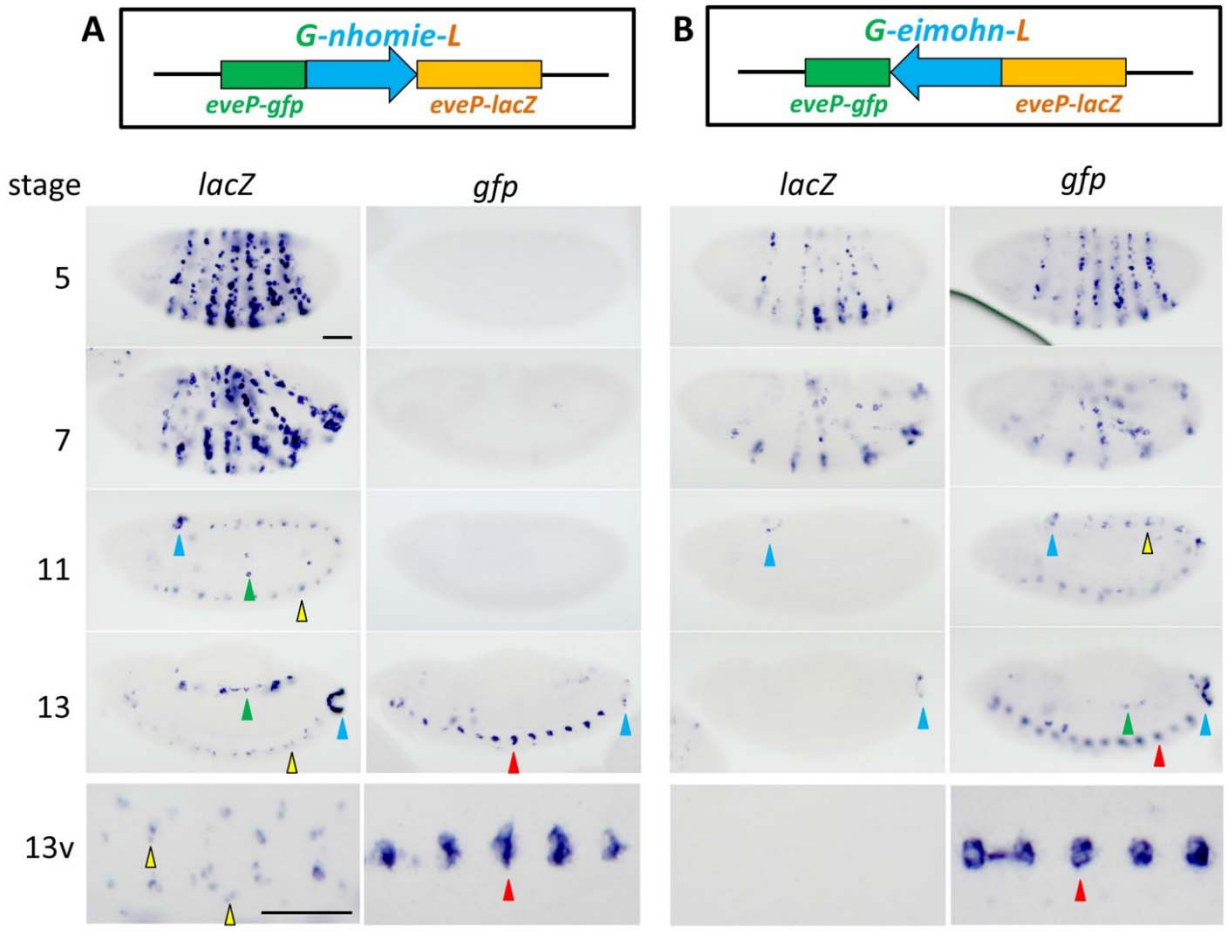

Figure 1-figure supplemental 1 Digoxigenin *in situs* showing expression of *lacZ* and GFP mRNAs from the *G-nhomie-L* (A) and *G-eimohn-L* (B) transgenes.

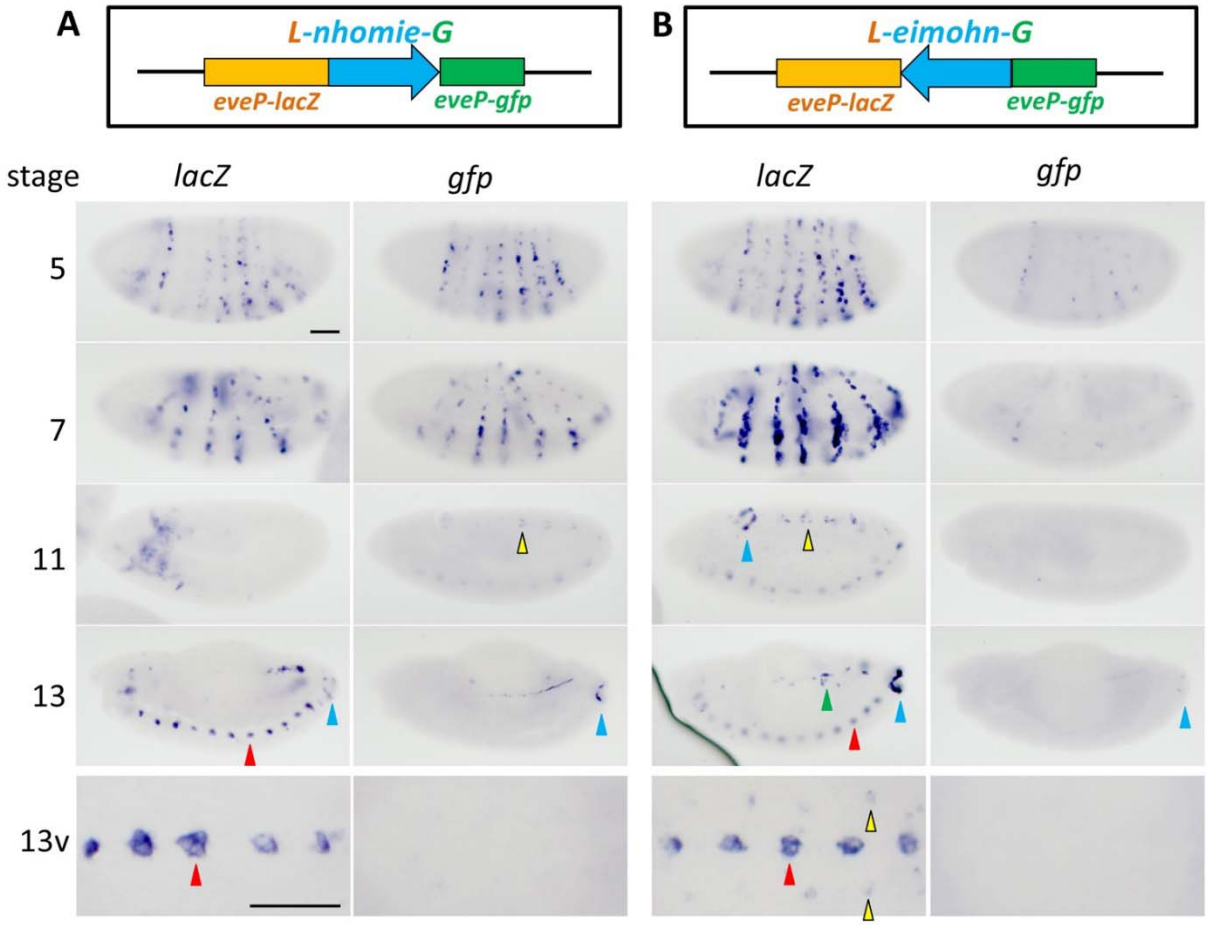

Figure 1-figure supplemental 2 Digoxigenin *in situs* showing expression of *lacZ* and GFP mRNAs from the *L-nhomie-G* (A) and *L-eimohn-G* (B) transgenes.

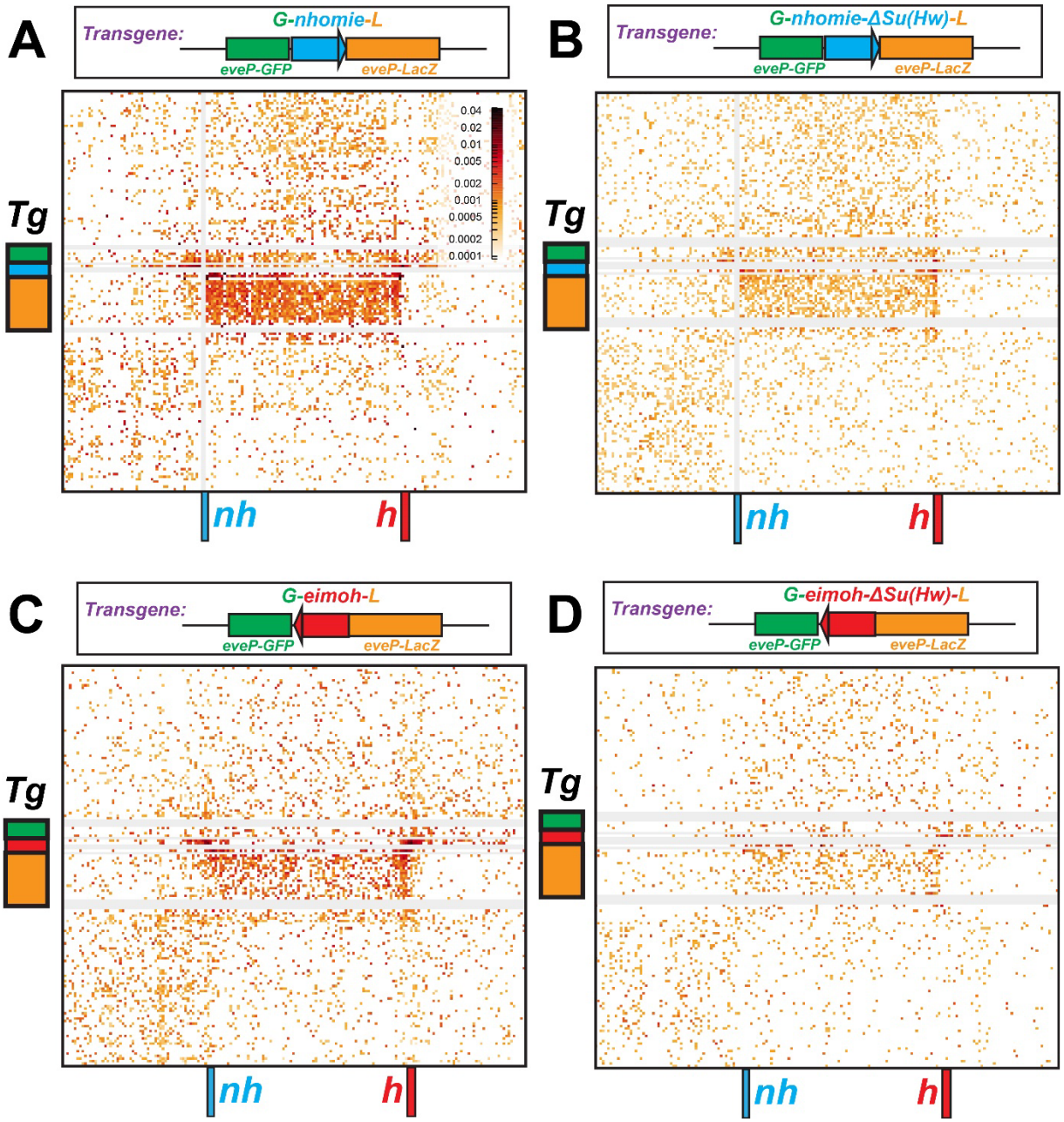

Figure 7-figure supplemental 1. Blow up of the MicroC interaction profiles between transgenes inserted at -142 kb and the *eve* TAD and TADs flanking the *eve* TAD.

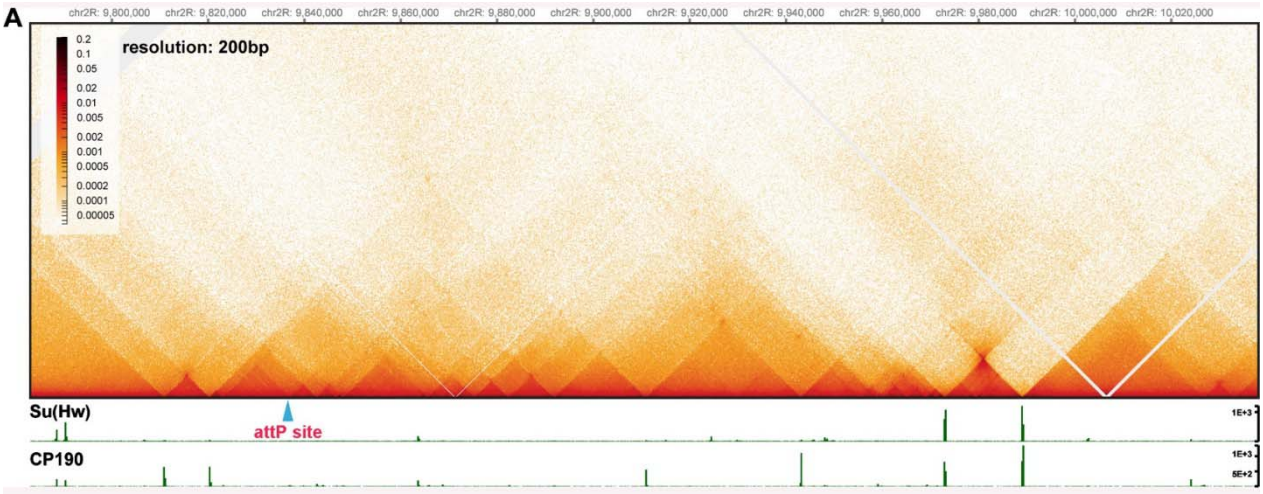

Figure 7-figure supplemental 2. Su(Hw) protein and TADs near the *hebe* attP site and the *eve* TAD

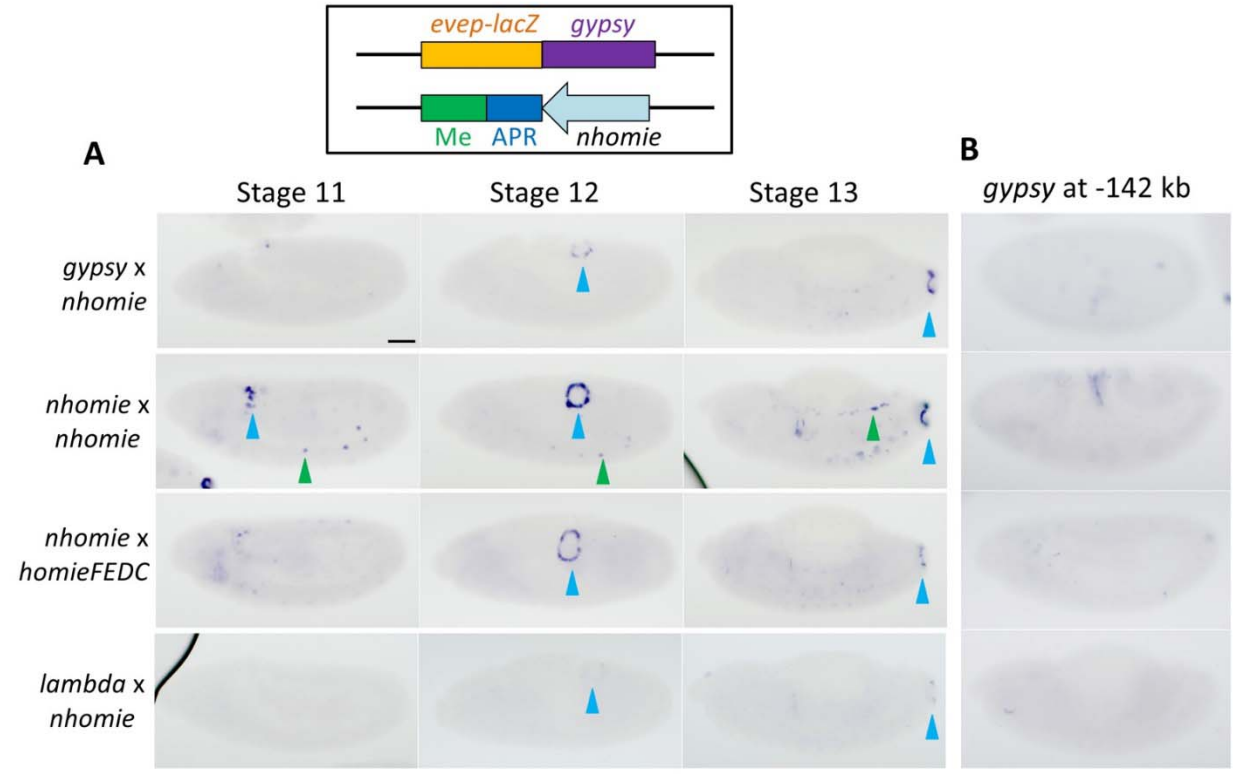

Figure 11 -figure supplemental 1. The su(Hw) *gypsy* insulator supports transvection with *nhomie*.

Figure Legends

Figure 1. Activation by *eve* enhancers of *nhomie*-containing transgenes inserted at -142 kb from *eve*. A. Map of *eve* locus, a subset of the intervening genes and the attP site in the first intron of the *hebe* gene. The three different transgene inserts oriented so that the *lacZ* reporter is closest to *eve* are shown: *lambda* DNA (*G-lambda-L*), *nhomie* in the same (forward) orientation as the *eve nhomie* (*G-nhomie-L*), and *nhomie* in the opposite (reverse) orientation as the *eve nhomie* (*G-eimohn-L*). B) The panels in each row show DAPI staining, *eve* mRNA, *gfp* mRNA, and *lacZ* mRNA for *G-lambda-L*, *G-nhomie-L* and *G-eimohn-L* blastoderm stage embryos. C) The panels in each row show DAPI staining, *eve* mRNA, *gfp* mRNA, and *lacZ* mRNA for *G-lambda-L*, *G-nhomie-L* and *G-eimohn-L* in stage 13-14 embryos. D) Quantitation of transgene expression (*lacZ* or *gfp*) for *G-lambda-L*, *G-nhomie-L*, and *G-eimohn-L* in stage 13-14 embryos.

Figure 2. *nhomie*-containing transgenes physically interact with the *eve* TAD. A) Top panel shows the MicroC contact profile in the wild-type chromosomal segment that contains both the insertion site (in the *hebe* gene) and the *eve* TAD. Bottom panels show blowups of the MicroC contact profile for the vicinity of the attP site in the *hebe* gene and the *eve* TAD. Note that the MicroC contact profile for the *eve* TAD has the characteristic signature of a stem-loop TAD—a plume above the volcano triangle. B) and C) MicroC contact profile and blow up for the *G-lambda-L* transgene. D) and E) MicroC contact profile and blowup for the *G-nhomie-L* transgene. Blue and green arrowheads indicate interactions between the *gfp* reporter and the TADs flanking the *eve* TAD. F) and G) MicroC contact profile and blow up for the *G-eimohn-L* transgene. Blue and green arrowheads indicate interactions between the *lacZ* reporter and the TADs flanking the *eve* TAD.

Figure 3. MicroC viewpoints from the *G-nhomie-L* and *G-eimohn-L* reporters. Viewpoints for the *G-nhomie-L* transgene for A) *gfp* and B) *lacZ* reporters. Viewpoints for the *G-eimohn-L* transgene for C) *gfp* and D) *lacZ* reporters. E) The average contact count per bin for the *gfp* and *lacZ* reporters, as indicated for the three transgene inserts *G-lambda-L*, *G-nhomie-L*, and *G-eimohn-L*. F) Models for chromatin organization of *G-nhomie-L* and *G-eimohn-L*.

Figure 4. Mutation of *nhomie* Su(Hw) binding site disrupts activation of transgene reporter expression by the *eve* enhancers. A) The panels in each row show DAPI staining, *eve* mRNA, *gfp* mRNA, and *lacZ* mRNA for *G-lambda-L*, *G-nhomie-L*, and *G-nhomieΔSu(Hw)-L* in blastoderm stage embryos. B) The panels in each row show DAPI staining, *eve* mRNA, *gfp* mRNA, and *lacZ* mRNA for *G-lambda-L*, *G-nhomie-L*, and *G-nhomieΔsu(Hw)-L* in stage13-14 embryos. C) Normalized maximum intensity projections of *gfp* and *lacZ* mRNA staining in the APR of stage13-14 embryos for each transgene.

Figure 5. Digoxigenin *in situ* hybridization in wild type and the Su(Hw) binding site mutants in *nhomie* and *homie*. Expression of the *lacZ* reporter by A) *G-nhomie-L*, B) *G-nhomieΔSu(Hw)-L*, C) *G-eimoh-L*, D) *G-eimohΔSu(Hw)-L*, and E) *G-lambda-L* transgene inserts are shown. The transgene constructs are illustrated on the top. Embryonic stages 5, 7, 11, 13 are shown. Ventral views of stage 13 (13v) are shown in the bottom row. Arrowheads indicate the following: blue: APR, yellow: *eve*-expressing neuronal cells, green: *eve*-expressing mesodermal cells, and red: *hebe*-expressing midline cell clusters. Scale bar: 50μm.

Figure 6. Mutation of the *homie* Su(Hw) binding site disrupts activation of transgene reporter expression by *eve* enhancers. A) The panels in each row show DAPI staining, *eve* mRNA, *gfp* mRNA, and *lacZ* mRNA for *G-lambda-L*, *G-eimoh-L*, and *G-eimohΔSu(Hw)-L* in blastoderm stage embryos. B) The panels in each row show DAPI staining, *eve* mRNA, *gfp* mRNA, and *lacZ* mRNA for *G-lambda-L*, *G-eimoh-L*, and *G-eimohΔSu(Hw)-L* in stage 13-14 embryos. C) Normalized maximum intensity projections of *gfp* and *lacZ* mRNA staining in the APR of stage 13-14 embryos for each transgene.

Figure 7. Mutation of the *nhomie* Su(Hw) binding site disrupts physical interactions between the transgene and sequences in the *eve* TAD. The MicroC contact profile and blow up for A) *G-nhomie-L* and B) *G-nhomieΔSu(Hw)-L* transgenes. Viewpoints from the *gfp* and *lacZ* reporters in C) *G-nhomie-L* and D) *G-nhomieΔSu(Hw)-L* transgenes. E) Average contact count per bin for the *gfp* and *lacZ* reporters, as indicated for the two transgene inserts *G-nhomie-L* and *G-nhomieΔSu(Hw)-L*. F) Insulation score for the transgene boundaries *nhomie* and *nhomieΔSu(Hw)*.

Figure 8. Mutation of the *homie* Su(Hw) binding site disrupts physical interactions between the transgene and sequences in the *eve* TAD. MicroC contact profile and blow up for A) *G-eimoh-L* and B) *G-eimohΔSu(Hw)-L* transgenes. Viewpoints from the *gfp* and *lacZ* reporters in C) *G-eimoh-L* and D) *G-eimohΔSu(Hw)-L* transgenes. E) Average contact count per bin for the *gfp* and *lacZ* reporters, as indicated for the two transgene inserts *G-eimoh-L* and *G-eimohΔSu(Hw)-L*. F) Insulation score for the transgene boundaries *eimoh* and *eimohΔSu(Hw)*.

Figure 9. Viewpoints from the transgene boundaries. A) *nhomie*, B) *nhomieΔSu(Hw)*, C) *eimoh*, and D) *eimohΔSu(Hw)*. Note the reduction in contacts between the Su(Hw) site mutant boundaries in the transgene and both *nhomie* and *homie* (at the ends of the *eve* TAD).

Figure 10. *homie*-dependent transvection is weakened by loss of the Su(Hw) binding site. Digoxigenin *in situ* hybridization showing *lacZ* expression in the transvection assay. The two transgene constructs used to assay transvection are illustrated at the top. The different transgene constructs used for each cross are indicated on the left as: reporter x enhancer. The negative control has a 500 bp *lambda* DNA fragment. The 367 bp *homie* (*homieCDEF*), 271 bp *homie* (*homieDEF*), and the Su(Hw) site-mutated *homieDEF* (*DΔSuEF*) were tested. Stages 11, 12, and 13 are shown. Arrowheads indicate the following: blue: APR and green: mesoderm. Scale bar: 50μm.

Figure 11. The su(Hw) *gypsy* insulator supports transvection with *homie*. Digoxigenin *in situ* hybridization showing *lacZ* expression in the transvection assay. The two transgene constructs for each experiment are shown on the top. The transgene combinations used in each case are indicated as reporter x enhancer. The negative control has a 500 bp *lambda* DNA fragment. The 349 bp *gypsy* fragment and 367 bp *homie* (*homieCDEF* and *homieFEDC*) were tested. Note that the orientation of *homie* in *homieFEDC* is inverted in the transgene to test whether *gypsy* interaction with *homie* is orientation-dependent. Stages 11, 12, and 13 are shown. Arrowheads indicate the following: blue: APR and green: mesoderm. Scale bar: 50μm.

Figure supplemental

Figure 1-figure supplemental 1. Digoxigenin *in situ* hybridization **showing expression of *lacZ* and *gfp* mRNAs from the *G-nhomie-L* (A) and *G-eimohn-L* (B) transgenes.** The transgene constructs are illustrated on the top. Embryonic stages 5, 7, 11, 13 are shown. Ventral views of stage 13 (13v) are shown in the bottom row. Arrowheads indicate the following: blue: APR, yellow: *eve*-expressing neuronal cells, green: *eve*-expressing mesodermal cells, and red: *hebe*-expressing midline cell clusters. Scale bar: 50µm.

Figure 1-figure supplemental 2. Digoxigenin *in situ* hybridization **showing expression of *lacZ* and *gfp* mRNAs from the *L-nhomie-G* (A) and *L-eimohn-G* (B) transgenes.** The transgene constructs are illustrated on the top. Embryonic stages 5, 7, 11, 13 are shown. Ventral views of stage 13 (13v) are shown in the bottom row. Arrowheads indicate the following: blue: APR, yellow: *eve*-expressing neuronal cells, green: *eve*-expressing mesodermal cells, and red: *hebe*-expressing midline cell clusters. Scale bar: 50µm.

Figure 7-figure supplemental 1. Blow up of the MicroC interaction profiles between transgenes inserted at -142 kb and the *eve* TAD, and TADs flanking the *eve* TAD. A) *G-nhomie-L*, B) *G-nhomieΔSu(Hw)-L*, C) *G-eimoh-L*, and D) *G-eimohΔSu(Hw)-L*. The position of the transgene is indicated on the right, while the positions of the *nhomie* (*nh*) and *homie* (*h*) boundaries are indicated below.

Figure 7-figure supplemental 2. Su(Hw) protein and TADs near the *hebe* attP site and the *eve* TAD. Location of TADs and Su(Hw) protein in region containing the *hebe* attP site and the *eve* TAD. **Need references for ChIP data.**

Figure 11-figure supplemental 1. The Su(Hw)-binding *gypsy* insulator supports transvection with *nhomie*. A) Digoxigenin *in situ* hybridization showing expression of *lacZ* in the transvection assay. The *nhomie* and *gypsy* transgene constructs are illustrated at the top. The transgenes used are indicated as reporter x enhancer at the left. A 500 bp *lambda* DNA fragment was used as a negative control (*lambda*). The 349 bp *gypsy* insulator fragment (which contains multiple Su(Hw) binding sites) and 602 bp *nhomie*, as well as *homieFEDC*, were tested. Stages 11, 12, and 13 are shown. Arrowheads indicate the following: blue: APR and green: mesoderm. Scale bar: 50µm. B: Digoxigenin *in situ* hybridization of *lacZ* expression when the dual reporter inserted in the -142 kb attP site contains the 349 bp *gypsy* insulator fragment.

Materials and methods

Key resources table

REAGENT or RESOURCE	SOURCE	IDENTIFIER
Chemicals, peptides, and recombinant proteins		
n-Heptane	Fisher Chemical	O3008-4
Paraformaldehyde 20% solution, EM Grade	Electron Microscopy Sciences	15713-S
Formaldehyde, 16%, methanol free, Ultra Pure	Polysciences Inc	18814-10
PBS - Phosphate-Buffered Saline (10X) pH 7.4, RNase-free	Thermo Fisher	AM9624
Tween 20	Sigma	P1379
Triton X-100	Bio-Rad	161-0407
Tris base	Sigma	11814273001
Methanol	Fisher Chemical	203403
SSC, 20X	Thermo Fisher	15557044
Formamide	Thermo Fisher	17899
Dextran sulfate	Sigma	D8906
Salmon Sperm DNA	Thermo Fisher	AM9680
Ribonucleoside Vanadyl Complex	NEB	S1402S
Nuclease-free BSA	Sigma	126609
Triethylammonium Acetate	Sigma	625718
dGTP (100 MM)	VWR	76510-208
dTTP (100 MM)	VWR	76510-224
Lonza NuSieve 3:1 Agarose	Thermo Fisher	BMA50090
T4 DNA ligase	NEB	M0202L
Biotin-11-dCTP	Jena Bioscience	NU-809-BIOX
Biotin-14-dATP	Jena Bioscience	NU-835-BIO14
Qubit dsDNA HS Assay Kit	Life Technologies Corp.	Q32851

Atto 633 NHS ester	Sigma	01464
Phase Lock Gel™, QuantaBio - 2302830, Phase Lock Gel Heavy	VMR	10847-802
NEBNext Ultra II DNA Library Prep Kit for Illumina	NEB	E7645S
Ampure Xp 5ml Kit	Thermo Fisher	NC9959336
Hifi Hotstart Ready Mix	Thermo Fisher	501965217
Dynabeads MyOne Streptavidin C1	Life Technologies Corp.	65001
cOmplete™, EDTA-free Protease Inhibitor Cocktail	Sigma	11873580001
N,N-Dimethylformamide	Sigma	227056
Potassium acetate solution	Sigma	95843
DSG (disuccinimidyl glutarate)	Thermo Fisher	PI20593
T4 Polynucleotide Kinase - 500 units	NEB	M0201S
DNA Polymerase I, Large (Klenow) Fragment - 1000 units	NEB	M0210L
End-it DNA End Repair Kit	Thermo Fisher	NC0105678
Proteinase K recomb. 100 mg	Sigma	3115879001
Nuclease MicroCoccal (s7)	Thermo Fisher	NC9391488
EGS (ethylene glycol bis(succinimidyl succinate))	Thermo Fisher	PI21565
Atto 565 NHS ester	Sigma	72464
HCR™ RNA-FISH Custom Probe Set: eve	Molecular Instruments	
HCR™ RNA-FISH Custom Probe Set: ter94	Molecular Instruments	
HCR™ RNA-FISH Custom Probe Set: CG12134	Molecular Instruments	
HCR™ RNA-FISH Custom Probe Set: eIF3j	Molecular Instruments	
HCR™ Amplifier B1, 488	Molecular Instruments	
HCR™ Amplifier B2, 564	Molecular Instruments	
HCR™ Amplifier B3, 647	Molecular Instruments	

HCR™ Buffers	Molecular Instruments	
NEBNext Multiplex Oligos for Illumina	NEB	E7335S
Software and algorithms		
Fiji (ImageJ)	Schindelin et al. (Schindelin et al. 2012)	fiji.sc

Plasmid construction and transgenic lines

The dual reporters construct was described previously (Fujioka et al. 2016). In short, each reporter contains the *eve* basal promoter (-275 to +106 bp relative to *eve* start site), either the *lacZ* (*eve-lacZ*) or *EGFP* (*eve-gfp*) coding region, and the *eve* 3' UTR (+1300 to +1525 bp). These two reporters are divergently transcribed. Test fragments were then inserted between the two reporters. The fragments used here are: a 500 bp fragment from *lambda* phage DNA, a 367 bp wild-type or Su(Hw)-mutant *homie* fragment (CDEF) (Fujioka et al., 2025), and a 602 bp wild-type or Su(Hw)-mutant *nhomie* fragment.

The -142 kb attP landing site was described previously (Fujioka et al. 2009). It contains two attP target sites for phiC31 recombinase-mediated cassette exchange (RMCE) (Bateman et al. 2006) and *mini-white* as a marker. RMCE can result in the insertion of the transgene in either orientation, and all four possible insertions of the transgenes can be recovered. For the experiments in this paper, we analyzed all four possible insertions for transgenes containing the *nhomie* fragment. For two of these, *G-eimohn-L* and *G-nhomie-L*, the *eve-lacZ* reporter is on the *eve* side of transgene *nhomie*, while *eve-gfp* is on the *hebe* enhancer side of the transgene *homie*. For the other two, *L-eimohn-G* and *L-nhomie-G*, the *eve-gfp* reporter is on the *eve* side of transgene *homie*, while *eve-lacZ* is on the *hebe* enhancer side of the transgene *nhomie*. For the *nhomie* Su(Hw) mutant *nhomie*Δ*SH*, we analyzed the *G-nhomie*Δ*SH-L* insert, where the *eve-lacZ* reporter is on the *eve* side of the transgene. For the two *homie* transgenes that were analyzed, *G-eimoh-L* and *G-eimoh*Δ*SH-L* the *eve-lacZ* reporter is also on the *eve* side of the transgene. RCMC events were identified by loss of *mini-white*, and the orientation of each insert was determined by PCR.

Two transgenes were used for the transvection assay (Fujioka et al., 2016). The reporter transgenes are the same ones used in -142 kb assay described above. For enhancer transgenes,

modified boundaries (described in figures) were flanked by the anal plate ring (APR) - mesodermal enhancers and two neuronal enhancers. The transvection assay was carried out so that *lacZ* in the dual reporter transgene and the APR-mesodermal enhancers was placed on the same side of the boundary. With this arrangement, *lacZ* is activated by APR and mesodermal enhancers. As described in the text, modified *homie*, nhomie, *lambda* DNA, and *gypsy* were inserted into these transgenes. The *homie* DNAs were the 367 bp CDEF fragment, the 271 bp DEF fragment and the Su(Hw) mutant fragment DΔSuEF (Fujioka et al., 2025). The *lambda* DNA and *gypsy* fragments were also described previously (2025).

HCR-FISH and digoxigenin *in situ* procedure

The sequences of target genes were obtained from Flybase (flybase.org)(Gramates et al. 2022). To design probes, the target gene sequences were submitted to the Molecular Instruments probe design platform (www.molecularinstruments.com/hcr-rnafish) (Choi et al. 2016), with parameters set to a 35 probe set size for *Drosophila melanogaster*. A similar method was designed based on published smFISH methods (Little and Gregor 2018; Trcek et al. 2017). 100-200 flies were placed in a cage with an apple juice plate at the bottom of the cage. For early stages, the embryos were collected for 7 hours at room temperature, while for later-stage embryos, collections were overnight. Embryos from each plate were washed into collection mesh and dechorionated in bleach for 2min, then fixed in 5mL of 4% paraformaldehyde in 1X PBS and 5mL of heptane for 15min with horizontal shaking. The paraformaldehyde was then removed and replaced with 5mL methanol. The embryos were then devitellinized by vortexing for 30s, and washed in 1mL of methanol twice. Methanol was then removed and replaced by PTw (1X PBS with 0.1% Tween-20) through serial dilutions of 7:3, 1:1, and 3:7 methanol:PTw. The embryos were washed twice in 1mL of PTw and pre-hybridized in 200µL of probe hybridization buffer for 30min at 37°C. 0.4pmol of each probe set were added to the embryos in probe hybridization buffer, and the embryos were incubated at 37^{o}C for 12-14h. The embryos were then washed 3X with probe wash buffer at 37°C for 30min and 2X with 5X SSCT(5X SSC+0.1% tween) at room temperature for 5min. Then the embryos were pre-amplified with 300µL amplification buffer for 10min at 25°C. Meanwhile, 6pmol of hairpin h1 and h2 were snap-cooled separately (95^{o}C for 90s, cool to RT with a 0.1^{o}C drop per second), and then mixed in 100µL of amplification buffer at room temperature. After that, the pre-amplification solution

was removed from the embryos, and 100µL of hairpin h1/h2 mix were added to the embryos. Next, the embryos were incubated for 12-14h at room temperature in the dark. To remove excess hairpins, the embryos were washed in SSCT as follows: 2X for 5min, 2X for 30min, and 5X for 5min. Then, the embryos were washed with 1mL PTw for 2min and stained with DAPI/Hoechst at 1µg/mL for 15min at room temperature in the dark. The embryos were then washed with PTw 3X for 5min. Finally, the embryos were mounted on microscope slides with Vectashield and a #1.5 coverslip for imaging.

The procedure for digoxigenin *in situ* was described previously (Fujioka et al. 2025).

Imaging, image analysis, and statistics

Embryos from HCR-FISH were imaged using a Nikon A1 confocal microscope system, with a Plan Apo 20X/0.75 DIC objective. Z-stack images were taken at interval of 2µm, 4X average, 1024x1024 resolution, and the appropriate laser power and gain were set for the 405, 488, 561, and 640 channels to avoid overexposure. Images were processed by ImageJ, and the maximum projection was applied to each of the stack images. To determine the presence of stripes in early embryos, multi-channel images were first split into single channels, and the stripe signal was then highlighted and detected by the MaxEntropy thresholding method. GraphPad Prism was used for data visualization and statistical analysis. Two-way ANOVA with Tukey's multiple comparisons test for each pair of groups was used to determine the statistical significance for the percentage of embryos carrying stripes in *eIF3j* and *TER94* channels in each group.

Imaging, image analysis and statistics

Embryos from smFISH were imaged using a Nikon A1 confocal microscope system with a Plan Apo 20X/0.75 DIC objective. Z-stack images were taken at intervals of 2µm, 4X average, 1024x1024 resolution, and the appropriate laser power and gain were set for the 405, 561, and 640 channels to avoid overexposure. Images were processed using ImageJ, and the maximum projection was applied to each of the stack images. To measure the stripe intensity of early embryos, multi-channel images were first split into single channels, and the stripe signal was then highlighted and selected by the MaxEntropy thresholding method. For APR intensity measurements, the ROI tool was used to crop out the APR region of late-stage embryos. The cells with APR signal were also highlighted and selected by MaxEntropy thresholding. The particle measurement tool was used to measure the average intensity of all cells that had a signal.

At the same time, the background signal (average intensity) was taken from cells without a signal in the same embryo. The relative intensity (signal to background) for each embryo was calculated using the stripe signal and background from the same embryo. To make comparisons between independent biological replicates, the average background signal of all embryos from each replicate was calculated. The relative intensity of each embryo from each replicate was normalized based on the average background signal of all embryos from that replicate. GraphPad Prism was used for data visualization and statistical analysis. To compare intensity from embryos in different groups, different signals from the same embryo (e.g., *lacZ* and *GFP*) were paired, and paired two-tailed t-tests were used to calculate p-values. All raw measurements and normalized data are included in Supplemental Data S2.

MicroC library construction

Embryos were collected on yeasted apple juice plates in population cages for 4 hours, incubated for 12hr at 25□, then subjected to fixation as follows. Embryos were dechorionated for 2min in 3% sodium hypochlorite, rinsed with deionized water, and transferred to glass vials containing 5 mL PBST (0.1% Triton-X100 in PBS), 7.5 mL n-heptane, and 1.5mL fresh 16% formaldehyde. Crosslinking was carried out at room temperature for exactly 15min on an orbital shaker at 250rpm, followed by addition of 3.7 mL 2M Tris-HCl pH7.5 and shaking for 5min to quench the reaction. Embryos were washed twice with 15 mL PBST and subjected to secondary crosslinking. Secondary crosslinking was done in 10mL of freshly prepared 3mM final DSG and ESG in PBST for 45 min. at room temperature with passive mixing. The reaction was quenched by addition of 3.7mL 2M Tris-HCl pH7.5 for 5min, washed twice with PBST, snap-frozen, and stored at -80□ until library construction.

Micro-C libraries were prepared as previously described (Batut et al. 2022) with the following modifications: 50uL of 12-16hr embryos were used for each biological replicate. 60U of MNase were used for each reaction to digest chromatin to a mononucleosome:dinucleosome ratio of 4. Libraries were barcoded, pooled, and subjected to paired-end sequencing on an Illumina Novaseq S1 100 nt Flowcell (read length 50 bases per mate, 6-base index read).

Micro-C data processing

MicroC data for *D. melanogaster* were aligned to custom genomes edited from the Berkeley Drosophila Genome Project (BDGP) Release 6 reference assembly (dos Santos et al. 2015) with

BWA-MEM (Li and Durbin 2009) using parameters **-S -P -5 -M**. Briefly, the custom genomes are simply insertions of the transgenic sequence into the –142kb integration site, as predicted from perfect integration. These events were confirmed using PCR post-integration. The resultant BAM files were parsed, sorted, de-duplicated, filtered, and split with Pairtools (https://github.com/mirnylab/pairtools). We removed pairs where only half of the pair could be mapped, or where the MAPQ score was less than three. The resultant files were indexed with Pairix (https://github.com/4dn-dcic/pairix). The files from replicates were merged with Pairtools before generating 100bp contact matrices using Cooler (Abdennur and Mirny 2020). Finally, balancing and Mcool file generation was performed with Cooler's Zoomify tool.

Virtual 4C profiles were extracted from individual replicates using FAN-C (Kruse et al. 2020) at 400bp resolution. The values were summed across replicates and smoothed across three bins (1.2kb). Viewpoints were determined based on the most informative region for interpretation. We used an 800bp window located downstream of the *eve* promoter, in the gene body of either *gfp* or *lacZ*. For the *nhomie* and *homie* viewpoints, the 800 bp window centered on the boundary; however, due to the masking of the duplicated boundary and *eve* promoters in the data analysis, a reduced signal is expected (Fig. 9).

Calculation and comparison of the insulation score at the *hebe* insertion site

We used the FAN-C (https://github.com/vaquerizaslab/fanc/tree/main) package to compute insulation scores on the merged Mcool maps corresponding to all the conditions, using a window size of 4 kb. The insulation score is defined as the log (base 2)-fold change between the signal within a 4 kb window centered on a site over the mean of all signal values along chromosome 2R. First, we computed boundaries using the boundary calling tool from FAN-C and identified the *hebe* insertion site for all mutants. Using these centered coordinates, we computed the insulation score at the *hebe* insertion site from the balanced contact maps. We then normalized this score relative to the local region around the *hebe* insertion site by subtracting the original insulation score from the mean of the insulation scores in a 40.2 kb window centered around the *hebe* insertion site. This mean-scaled normalization can be interpreted as the level of insulation at the *hebe* insertion relative to its local neighborhood. We computed the change in the normalized insulation between *G-lambda-L* and all mutants.

Quantification of total contacts between the *hebe* transgene reporter and the *eve* locus

For all the mutants, we identified the location of the *hebe* locus and the *eve* locus (specifically, the region between *nhomie* and *homie*). We then visualized the interaction region between the *hebe* insertion and the *eve* locus to manually segment bounding boxes of interaction between the *lacZ* reporter and the *eve* locus. After matrix balancing and masking of null values, we took the mean of the contact frequencies within this bounding box for each dataset. This became the average contact frequency between *lacZ* and *hebe* transgene. We repeated this procedure for *gfp*.

Data availability

Sequence data are available at GSE330020. Analysis and notes are available at https://github.com/pritykinlab/suhw-tad-boundary-mechanisms.

Acknowledgements: Part of this work was supported by NIH grants to Paul Schedl (5R35GM126975), to James B. Jaynes (1R01GM137062) and to Yuri Pritykin (DP2AI171161). Princeton Bioengineering Biocondensates Program to Yuri, and a New Jersey Commission on Cancer Research (COCR23PDF011) to Wenfan Ke. Authors would like to thank Gordon Grey for preparing fly food, members of the Lewis Sigler Genomics Core facility for the assistance with DNA sequencing and Qing Liu for excellent technical assistance.

References

AlHaj Abed J, Erceg J, Goloborodko A, Nguyen SC, McCole RB, Saylor W, Fudenberg G, Lajoie BR, Dekker J, Mirny LA, Wu CT. (2019). Highly structure homolog pairing reflects functional organization of the Drosophila genome. Nat Commun. 2019 Oct 3;10(1):4485. doi: 10.1038/s41467-019-12208-3.PMID: 31582763

Aoki T, Sarkeshik A, Yates J, Schedl P.(2012). Elba, a novel developmentally regulated chromatin boundary factor is a heterotripartite DNA binding complex Elife. 2012 Dec 13;1:e00171. doi: 10.7554/eLife.00171.PMID: 23240086

Avva SV, Hart CM. 2016. Characterization of the drosophila beaf-32a and beaf-32b insulator proteins. PLoS One. 11(9):e0162906

Batut PJ, Bing XY, Sisco Z, Raimundo J, Levo M, Levine MS. 2022. Genome organization controls transcriptional dynamics during development. Science. 375(6580):566-570. doi: 10.1126/science.abi7178. Epub 2022 Feb 3.PMID: 35113722

Bing X, Ke W, Fujioka M, Kurbidaeva A, Levitt S, Levine M, Schedl P, Jaynes JB. (2024) Chromosome structure in Drosophila is determined by boundary pairing not loop extrusion. Elife. 2024 Aug 7;13:RP94070. doi: 10.7554/eLife.94070.PMID: 39110499

Blanton J, Gaszner M, Schedl P.(2003). Protein:protein interactions and the pairing of boundary elements in vivo. Genes Dev. 2003 Mar 1;17(5):664-75. doi: 10.1101/gad.1052003.PMID: 12629048

Bonchuk A, Denisov S, Georgiev P, Maksimenko O.(2011). Drosophila BTB/POZ domains of the “ttk group” can form multimers and selectively interact with each other. J Mol Biol. 2011 Sep 23;412(3):423-36. doi: 10.1016/j.jmb.2011.07.052. Epub 2011 Jul 29.PMID: 21821048

Bonchuk A, Boyko K, Fedotova A, Nikolaeva A, Lushchekina S, Khrustaleva A, Popov V, Georgiev P. (2021) Structural basis of diversity and homodimerization specificity of zinc finger associated domains in Drosophila. .Nucleic Acids Res. Feb 26;49(4):2375-2389. doi: 10.1093/nar/gkab061.PMID: 33638995

Bonchuk A, Balagurov K, Georgiev P. (2023) BTB domains: a structural view of evolution, multimerization and protein:protein interactions. Bioessays. Feb;45(2):e2200179. doi: 10.1002/bies.202200179. Epub 2022 Nov 30.PMID: 36449605

Cai HN, Shen P. (2001). Effects of cis arrangement of chromatin insulators on enhancer blocking activity. Science. 291:493-5. doi: 10.1126/science.291.5503.493. PMID: 11161205

Callan HG (1986) Lampbrush chromosomes. Mol. Biol Biochem. Biophys 36:1-252. Springer, Berlin. PMID: 3531807

Callan HG. (1987) Lampbrush chromsomes as seen in historical perspective. Results Probl Cell Differ. 1987;14:5-26. doi: 10.1007/978-3-540-47783-9_2.PMID: 3303217

Cavalheiro GR, Pollex T, Furlong EE. 2021. To loop or not to loop: What is the role of tads in enhancer function and gene regulation? Curr Opin Genet Dev. 67:119-129. doi: 10.1016/j.gde.2020.12.015. Epub 2021 Jan 23.PMID: 33497970

Chetverina D, Fujioka M, Erokhin M, Georgiev P, Jaynes JB, and Schedl P (2017) Boundaries of loop domains (insulators): Determinants of chromosome form and function in multicellular eukaryotes. Bioessays. 2017 Mar;39(3). doi: 10.1002/bies.201600233. Epub 2017 Jan 30. PMID:28133765 PMC5536339.

Chetverina D, Erokhin M, Schedl P. (2021) GAGA factor: a multifunctional pioneering chromatin protein. Cell Mol Life Sci. 2021 May;78(9):4125-4141. doi: 10.1007/s00018-021-03776-z. Epub 2021 Feb 2.PMID: 33528710

Child MB 6th, Bateman JR, Jahangiri A, Reimer A, Lammers NC, Sabouni N, Villamarin D, McKenzie-Smith GC, Johnson JE, Jost D, Garcia HG.(2021). Live imaging and biophysical modeling support a button based mechanism of somatic homolog pairing in Drosophila. Elife. 2021 Jun 8;10:e64412. doi: 10.7554/eLife.64412.PMID: 34100718

Cuartero S, Fresán U, Reina O, Planet E, Espinàs ML.I2014). Ibf1 and Ibf2 are novel CP190 interacting proteins required for insulator function. EMBO J. 2014 Mar 18;33(6):637-47. doi: 10.1002/embj.201386001. Epub 2014 Feb 6.PMID: 24502977

Dai Q, Ren A, Westholm JO, Serganov AA, Patel DJ, Lai EC. (2013) The BEN domain is a novel sequence specific DNA binding domain conserved in neural transcriptional repressors. Genes Dev. 2013 Mar 15;27(6):602-14. doi: 10.1101/gad.213314.113. Epub 2013 Mar 6.PMID: 23468431

Davidson, I.F., and Peters, J.M. (2021). Genome folding through loop extrusion by SMC complexes. Nat. Rev. Mol. Cell Biol. 22, 445–464. https://doi.org/10.1038/s41580-021-00349-7.

Dekker J, Heard E. (2016) Stuctural and functional diversity of topologically associating domains FEBS Lett. 2015 Oct 7;589(20 Pt A):2877-84. doi: 10.1016/j.febslet.2015.08.044. Epub 2015 Sep 5.PMID: 26348399

Dekker J, Mirny LA. (2024) The chromosome folding problem and how cells solve it Cell. 2024 Nov 14;187(23):6424-6450. doi: 10.1016/j.cell.2024.10.026.PMID: 39547207

Dixon JR, Selvaraj S, Yue F, Kim A, Li Y, Shen Y, Hu M, Liu JS, Ren B. (2012) Topological domains in mammalian genomes identified by analysis of chromatin interactions Nature. 2012 Apr 11;485(7398):376-80. doi: 10.1038/nature11082.PMID: 22495300

Dolsten GA, Cofer EM, Bing XY, Brack B, Curlin M, Theesfeld CL, Troyanskaya OG, Levine MS, Pritykin Y. (2025) 3D chromatin structures precede genome activation in Drosophila embryogenesis. Cell Genom. 2025 Nov 12;5(11):101002. doi: 10.1016/j.xgen.2025.101002. Epub 2025 Sep 15.PMID: 40957418

Eagen KP, Hartl TA, Kornberg RD. (2015) Stable chromosome condensation revealed by chromosome conformation capture. Cell. 2015 Nov 5;163(4):934-46. doi: 10.1016/j.cell.2015.10.026.PMID: 26544940

Fedotova AA, Bonchuk AN, Mogila VA, Georgiev PG. (2017). C2H2 zinc finger proteins: the largest but poorly explored family of higher eukaryotic transcription factors .Acta Naturae. 2017 Apr-Jun;9(2):47-58.PMID: 28740726

Fujioka M, Wu X, Jaynes JB. (2009) A chromatin insulator mediates transgene homing and very long-range enhancer-promoter communication. Development. 2009 Sep;136(18):3077-87. doi: 10.1242/dev.036467. Epub 2009 Aug 12.PMID: 19675129

Fujioka M, Mistry H, Schedl P, Jaynes JB. (2016). Determinants of chromosome architecture: insulator pairing in cis and in trans. PLoS Genet. 2016 Feb 24;12(2):e1005889. doi: 10.1371/journal.pgen.1005889. eCollection 2016 Feb.PMID: 26910731

Fujioka M, Ke W, Schedl P, Jaynes JB. (2025) The homie insulator has sub-elements with different insulating and long range pairing properties. Genetics. 2025 Apr 17;229(4):iyaf032. doi: 10.1093/genetics/iyaf032.PMID: 39999387

Fudenberg G, Imakaev M, Lu C, Goloborodko A, Abdennur N, Mirny LA. (2016). Formation of chromosomal domains by loop extrusion. Cell Rep. 2016 May 31;15(9):2038-49. doi: 10.1016/j.celrep.2016.04.085. Epub 2016 May 19.PMID: 27210764

Gall JG, Callan HG. (1962). H^3 uridine incorporation in lampbrush chromosomes. Proc Natl Acad Sci U S A. 1962 Apr 15;48(4):562-70. doi: 10.1073/pnas.48.4.562.PMID: 13896377

Gasner, M., Vazquez, J. and Schedl, P. (1999) The *zw5* protein, a component of the *scs* chromatin domain boundary, is able to block enhancer promoter interactions. *Genes and Development* 13, 2098-2107 PMID: 10465787 doi: 10.1101/gad.13.16.2098.PMID: 10465787

Ghirlando R, Felsenfeld G.(2016). CTCF:making the right connections. Genes Dev. 2016 Apr 15;30(8):881-91. doi: 10.1101/gad.277863.116.PMID: 27083996

Ghirlando R, Giles K, Gowher H, Xiao T, Xu Z, Yao H, Felsenfeld G. (2012) Chromatin domains, insulators, and the regulation of gene expression. Biochim Biophys Acta. 2012 Jul;1819(7):644-51. doi: 10.1016/j.bbagrm.2012.01.016. Epub 2012 Feb 2.PMID: 22326678

Ghosh, D., Gerasimova, T. I. & Corces, V. G. (2001). Interactions between the Su(Hw) and Mod(mdg4) proteins required for gypsy insulator function. EMBO J. 20, 2518–2527 (2001) doi: 10.1093/emboj/20.10.2518.PMID: 11350941

Golovnin A, Mazur A, Kopantseva M, Kurshakova M, Gulak PV, Gilmore B, Whitfield WG, Geyer P, Pirrotta V, Georgiev P.(2007) Integrity of the Mod(mdg4)-67.2 BTB domain is critical to insulator function in Drosophila melanogaster. Mol Cell Biol. 2007 Feb;27(3):963-74. doi: 10.1128/MCB.00795-06. Epub 2006 Nov 13.PMID: 17101769

Golovnin A, Melnikova L, Babosha V, Pokholkova GV, Slovohotov I, Umnova A, Maksimenko O, Zhimulev IF, Georgiev P. The N-terminal part of Drosophila CP190 is a platform for interaction with multiple architectural proteins. Int J Mol Sci. 2023 Nov 2;24(21):15917. doi: 10.3390/ijms242115917.PMID: 37958900

Goel VY, Huseyin MK, Hansen AS.(2023) Region capture MicroC relveals coalesece of enhancers and promoters into nested microcompartments. Nat Genet. 2023 Jun;55(6):1048-1056. doi: 10.1038/s41588-023-01391-1. Epub 2023 May 8.PMID: 37157000

Gohl, D., Aoki, T., Blanton, J., Shanower, G., Kappes, G., and Schedl, P. (2011). Mechanism of boundary action: sink, barrier or loop? Genetics. 2011 Mar;187(3):731-48. doi: 10.1534/genetics.110.123752. Epub 2010 Dec 31.PMID: 21196526

Harrison, D. A., Gdula, D. A., Coyne, R. S. & Corces, V. G. (1993) A leucine zipper domain of the suppressor of Hairy-wing protein mediates its repressive effect on enhancer function. Genes Dev. 7, 1966–1978 (1993 doi: 10.1101/gad.7.10.1966.PMID: 7916729

Hsieh TS, Cattoglio C, Slobodyanyuk E, Hansen AS, Rando OJ, Tjian R, Darzacq X (2021). Resolving the 3D landscape of transcription linked mammalian chromatin folding. Mol Cell 78(3):539-553.e8. doi: 10.1016/j.molcel.2020.03.002. Epub 2020 Mar 25.PMID: 32213323

Kaushal A, Dorier J, Wang B, Mohana G, Taschner M, Cousin P, Waridel P, Iseli C, Semenova A, Restrepo S, Guex N, Aiden EL, Gambetta MC. Essential role of Cp190 in physical and regulatory boundary formation. Sci Adv. 2022 May 13;8(19):eabl8834. doi: 10.1126/sciadv.abl8834. Epub 2022 May 13.PMID: 35559678

Ke W, Fujioka M, Schedl P, Jaynes JB.(2024). Stem-loop and circle-loop TADs generated by directional pairing of boundary elments h ave distinct physical and regulatory properties. Elife. 2024 Aug 7;13:RP94114. doi: 10.7554/eLife.94114.PMID: 39110491

Kellum R, Schedl P. (1992) A group of scs elements function as domain boundaries in an enhancer-blocking assay. Mol Cell Biol. 1992 May;12(5):2424-31. doi: 10.1128/mcb.12.5.2424-2431.1992.PMID: 1569958

Kim, J., Shen, B., Rosen, C. & Dorsett, D. (1996). The DNA-binding and enhancer-blocking domains of the Drosophila suppressor of Hairywing protein. Mol Cell Biol. *16*, 3381–3392. doi: 10.1128/MCB.16.7.3381.PMID: 8668153

Kyrchanova O, Chetverina D, Maksimenko O, Kullyev A, Georgiev P.(2008a). Orientation-dependent interaction between Drosophila insulators is a property of this class of regulatory elements. Nucleic Acids Res. 36(22):7019-28. doi: 10.1093/nar/gkn781. Epub 2008 Nov 5. PMID: 18987002

Kyrchanova O, Toshchakov S, Podstreshnaya Y, Parshikov A, Georgiev P.(2008b) Functional interaction between the Fab-7 and Fab-8 boundaries and the upstream promoter region in the Drosophila Abd-B gene. Mol Cell Biol. 2008 Jun;28(12):4188-95. doi: 10.1128/MCB.00229-08. Epub 2008 Apr 21.PMID: 18426914

Kyrchanova O, Ivlieva T, Toshchakov S, Parshikov A, Maksimenko O, Georgiev P.(2011) Selective interactions of boundaries with upstream region of Abd-B promoter in Drosophila bithorax complex and role of dCTCF in this process. Nucleic Acids Res. 2011 Apr;39(8):3042-52. doi: 10.1093/nar/gkq1248. Epub 2010 Dec 10.PMID: 21149269

Krietenstein N, Abraham S, Venev SV, Abdennur N, Gibcus J, Hsieh TS, Parsi KM, Yang L, Maehr R, Mirny LA, Dekker J, Rando OJ. (2020). Ultrastructural details of mammalian chromosome architecture. Mol Cell. 78(3):554-565.e7. doi: 10.1016/j.molcel.2020.03.003. Epub 2020 Mar 25.PMID: 32213324

Levo M, Raimundo J, Bing XY, Sisco Z, Batut PJ, Ryabichko S, Gregor T, Levine MS. 2022.Transcriptional coupling of distant regulatory genes in living embryos. Nature. 605(7911):754-760. doi: 10.1038/s41586-022-04680-7. Epub 2022 May 4.PMID: 35508662

Li H-B, Muller M, Bahechar IA, Kyrchanova O, Ohno K, Georgiev P, Pirrotta V. 2011. Insulators, not polycomb response elements, are required for long-range interactions between polycomb targets in drosophila melanogaster. Mol Cell Biol. 31(4):616-625. doi: 10.1128/MCB.00849-10. Epub 2010 Dec 6.PMID: 21135119

Li M, Ma Z, Roy S, Patel SK, Lane DC, Duffy CR, Cai HN. (2018) Chromatin boundary elements organize genomic architecture and developmental gene regulation in Drosophila Hox clusters. Sci Rep. 2018 Oct 11;8(1):15158. doi: 10.1038/s41598-018-33588-4.PMID: 30310129

Maksimenko O, Bartkuhn M, Stakhov V, Herold M, Zolotarev N, Jox T, Buxa MK, Kirsch R, Bonchuk A, Fedotova A, Kyrchanova O, Renkawitz R, Georgiev P.I2015) Two new insulator proteins, Pita and zIPIC target CP190 to chromatin. Genome Res. 2015 Jan;25(1):89-99. doi: 10.1101/gr.174169.114. Epub 2014 Oct 23.PMID: 25342723

Melnikova L, Kostyuchenko M, Molodina V, Parshikov A, Georgiev P, Golovnin A. Multiple interactions are involved in a highly specific association of the Mod(mdg4)-67.2 isoform with the Su(Hw) sites in *Drosophila*. Open Biol. 2017 Oct;7(10):170150. doi: 10.1098/rsob.170150.PMID: 29021216

Melnikova L, Kostyuchenko M, Molodina V, Parshikov A, Georgiev P, Golovnin A. Interactions between BTB domain of CP190 and two adjacent regions in Su(Hw) are required for insulator complex formation. Chromosoma. 2018 Mar;127(1):59-71. doi: 10.1007/s00412-017-0645-6. Epub 2017 Sep 22.PMID: 28939920

Melnikova L, Elizar'ev P, Erokhin M, Molodina V, Chetverina D, Kostyuchenko M, Georgiev P, Golovnin A. The same domain of Su(Hw) is required for enhancer blocking and direct promoter repression. Sci Rep. 2019 Mar 29;9(1):5314. doi: 10.1038/s41598-019-41761-6.PMID: 30926937

Matthews NE, White R. (2019) Chromatin architecture in the fly: living without CTCF/cohesin loop extrusion? Alternating chromatin states provides a basis for domain architecture in Drosophila. Bioessays. 2019 Sep;41(9):e1900048. doi: 10.1002/bies.201900048. Epub 2019 Jul 1.PMID: 31264253

Muller, M., Gyurkovics, H., Hagstrom, K., Pirrotta, V and Schedl, P. (1999) The *Mcp* element from the Drosophila melanogaster bithorax complex mediates long-distance regulatory interactions. *Genetics* 153:1333-56. doi: 10.1093/genetics/153.3.1333. PMID: 10545463

Muravyova E, Golovnin A, Gracheva E, Parshikov A, Belenkaya T, Pirrotta V, Georgiev P. (2001). Loss of insulator activity by paired Su(Hw) chromatin insulators. Science. 2001 Jan 19;291(5503):495-8. DOI: 10.1126/science.291.5503.495.PMID: 11161206

Pai CY, Lei EP, Ghosh D, Corces VG. The centrosomal protein CP190 is a component of the gypsy chromatin insulator. Mol Cell. 2004 Dec 3;16(5):737-48. doi: 10.1016/j.molcel.2004.11.004.PMID: 15574329

Parkhurst SM, Harrison DA, Remington MP, Spana C, Kelley RL, Coyne RS, Corces VG. (1988) The Drosophila su(Hw) gene, which controls the phenotypic effects of the gypsy transposable element, encodes a putative DNA binding protein. Genes Dev. 1988 Oct;2(10):1205-15. doi: 10.1101/gad.2.10.1205.PMID: 2462523

Sigrist CJ, Pirrotta V. (1997). Chromatin insulator elements block the silencing of a target gene by the Drosophila polycomb response element (PRE) but allow trans interactions between PREs on different chromosomes. Genetics. Sep;147(1):209-21. doi: 10.1093/genetics/147.1.209.PMID: 9286681

Stadler, M.R.; Haines, J.E.; Eisen, M.B. Convergence of topological domain boundaries, insulators, and polytene interbands revealed by high-resolution mapping of chromatin contacts in the early Drosophila melanogaster embryo. *eLife* 2017, *6*, e29550

Rao SS, Huntley MH, Durand NC, Stamenova EK, Bochkov ID, Robinson JT, Sanborn AL, Machol I, Omer AD, Lander ES, Aiden EL. (2014). A 3D map of the human genome at kilobase resolutions reveals principles of chromatin looping. Cell. 2014 Dec 18;159(7):1665-80. doi: 10.1016/j.cell.2014.11.021. Epub 2014 Dec 11.PMID: 25497547

Rao, S.S.P., Huang, S.C., Glenn St Hilaire, B., Engreitz, J.M., Perez, E.M., Kieffer-Kwon, K.R., Sanborn, A.L., Johnstone, S.E., Bascom, G.D., et al.(2017). Cohesin Loss Eliminates All Loop Domains. Cell 171, 305–320.e24. https://doi.org/10.1016/j.cell.2017.09.026.

Vazquez, J., Farkas, G., Gaszner, M., Udvardy, A., Muller, M., Hagstrom, K., Gyurkovics, H., Sipos, L., Gausz, J., Galloni, M., Hogga, I., Karch, F., and Schedl, P. (1993) Genetic and molecular analysis of chromatin domains. Cold Spring Harbor Viets K, Sauria MEG, Chernoff C, Rodriguez Viales R, Echterling M, Anderson C, Tran S, Dove A, Goyal R, Voortman L, Gordus A, Furlong EEM, Taylor J, Johnston RJ Jr(2019), Characterization of button loci that promote homologous chromosome pairing and cell-type-specific interchromosomal gene regulation. .Dev Cell. 2019 Nov 4;51(3):341-356.e7. doi: 10.1016/j.devcel.2019.09.007. Epub 2019 Oct 10.PMID: 31607649

28;10(8):e1004544. doi: 10.1371/journal.pgen.1004544. eCollection 2014 Aug.PMID: 25165871

Zhao K, Hart CM, Laemmli UK.(1995) Visualization of chromosomal domains with the boundary element associated factor BEAF-52. Cell. 1995 Jun 16;81(6):879-89. doi: 10.1016/0092-8674(95)90008-x.PMID: 7781065

Zolotarev N, Fedotova A, Kyrchanova O, Bonchuk A, Penin AA, Lando AS, Eliseeva IA, Kulakovskiy IV, Maksimenko O, Georgiev P.(2016) Architectural protiens Pita, Zw5, and ZIPIC contain homodimerization domains and support specific long-range interactions in Drosophila. Nucleic Acids Res. 2016 Sep 6;44(15):7228-41. doi: 10.1093/nar/gkw371. Epub 2016 May 2.PMID: 27137890